ENR-IFE.02.CEA-01

Magnetized ICF

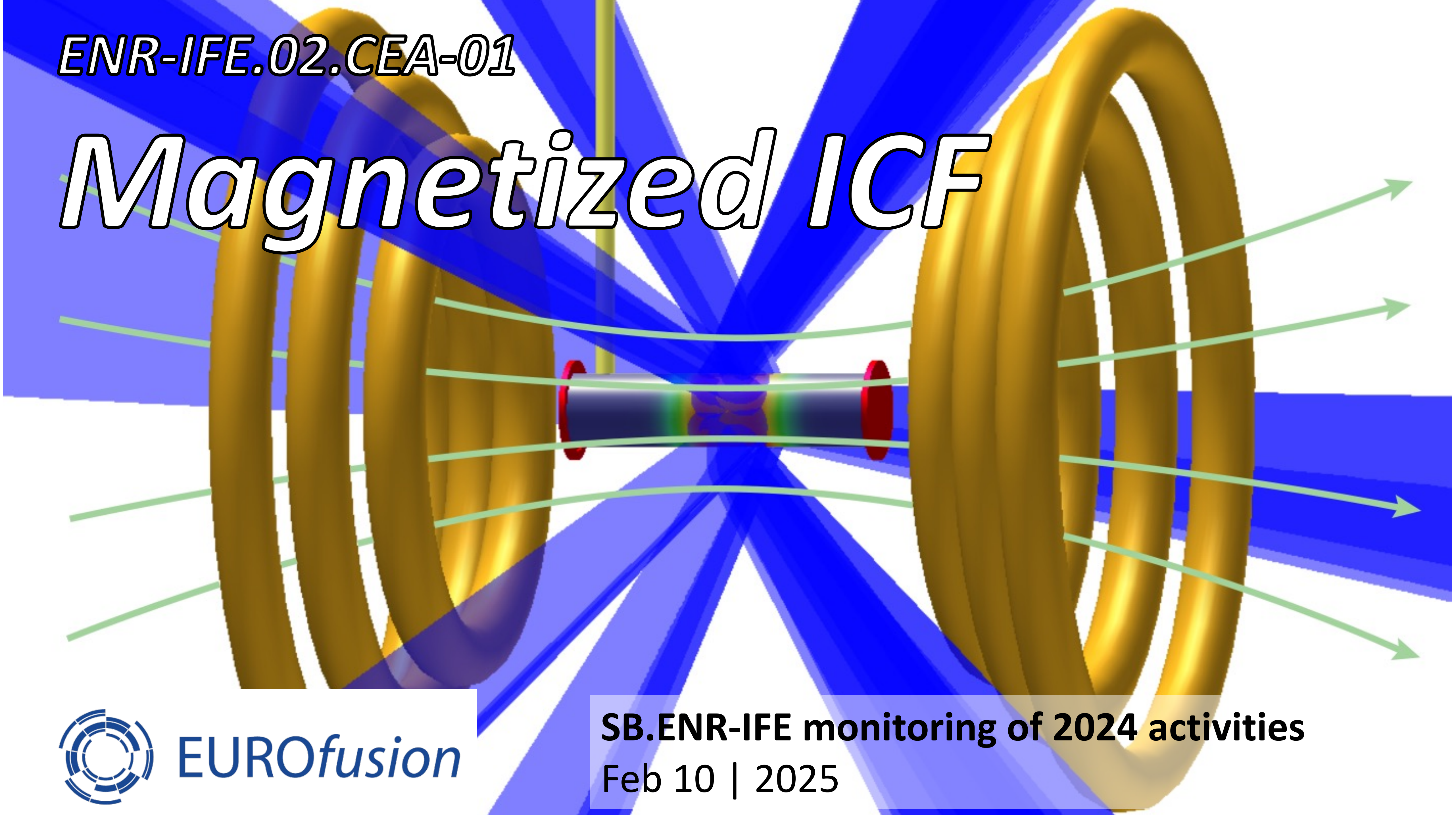

EUROfusion

SB.ENR-IFE monitoring of 2024 activities

Feb 10 | 2025

Objectives

Investigation of plasma processes underlying magnetized ICF for energy

Use of laser-based platforms for HED plasmas embedded in strong magnetic fields :

WP1 - Large scale implosion experiments (OMEGA, NIF, LMJ) focus on the extended-MHD effects on the transport of energy and magnetic flux

WP2 - Medium scale experiments (LULI, XFEL, …) focus on the microscopic (kinetic) physics of heat transport and diffusion of magnetic field

Experiments are combined with modelling efforts

- Radiative-hydrodynamic: *CHIC, TROLL*
- Extended-magnetohydrodynamic (MHD) codes: *HERA, FLASH, GORGON, CHIMERA*
- Vlasov-Fokker-Planck (VFP) kinetic codes: *Aladin*
- Molecular dynamics (DM): *BinGo-TCP, DinMol*
- Atomic physics and collision radiative models: *MERL, PPP-B, ABAKO, SAPHyR*

Participants

CELIA – Univ. Bordeaux
M. Bardon, M. Caetano de Sousa, B. Chimier,
A. Da Ros, N. Fefeu, Ph. Nicolaï, J.J. Santos, V.T. Tikhonchuk

LULI – Ecole Polytechnique
B. Albertazzi, D. Barlow, M. Koenig, J.-R. Marqués

PIIM – Aix-Marseille Univ.
S. Ferri, A. Calisti, J. Rosato, M. Koubiti, C. Mossé

CEA
P. Loiseau, C. Rousseaux

Univ. Rennes
J. Mathiaud

Univ. Las Palmas de Gran Canaria
A. Bordón, R. Florido

Univ. Valladolid
M.A. Gigosos, G. Pérez-Callejo

Univ. Politécnica Madrid - Aeronáuticos
J.J. Honrubia

CLPU – Univ. Salamanca
M. Ehret, J.L. Henares

ENEA
M. Alonzo, F. Consoli, F. Filippi, M. Sciscio

HMU
I. Fitilis, M. Tatarakis, I. Tazes, C. Vlachos

IPPLM
T. Chodukowski, Y. Domanski, H. Marchenko, T. Pisarczyk,
M. Rosinki, Z. Rusiniak, P. Tchórz, A. Zaras-Szydlowska

IPP.CR
J. Cikhardt

ICLondon
J. Chittenden, P. Maloney, C. Silva de Freitas, F. Suzuki-Vidal

Univ. York
N. Woolsey

STFC - UKRI
P. Bradford

Focused Energy
A. Debayle

Univ. California San Diego
M. Bailly-Grandvaux, F. Beg, E. Rovere

Univ. Nevada, Reno
R. Mancini

Lawrence Livermore Nat. Lab.
B. Pollock, C.A. Walsh

Los Alamos Nat. Lab.
W. Gammel, S. Palaniyappan, J. Sauppe

General Atomics
C. McGuffey

Magnetized ICF

Can magnetization further enhance fusion yields in ICF ?

Strong B-fields embedded in HED plasmas alter charged particles trajectories and change the way heat is transported

- Electron magnetization **reduces thermal conduction** losses from the hotspot perpendicularly to the B-field

$$\omega_{ce}\tau_e > 1 \implies B > 10^3 - 10^4 \text{ T}$$

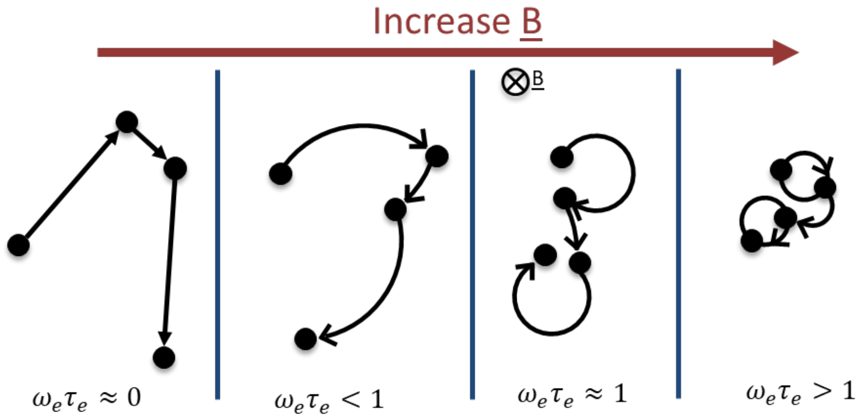

Hotspot self-heating condition :

Enhanced α heating

Reduced thermal losses

$$\frac{d\varepsilon_{HS}}{dt} = P_\alpha + P_{\text{pdV}} - P_\kappa - P_{\text{rad}} > 0$$

Mechanical work

Radiation losses

- Magnetic confinement of the α-particles enhances their path, therefore their collisionality within the hotspot, and **raises self-sustained fusion reactions yield** reducing the ρR requirements

$$r_L^\alpha < R_{core} \implies B > 10^4 - 10^5 \text{ T}$$

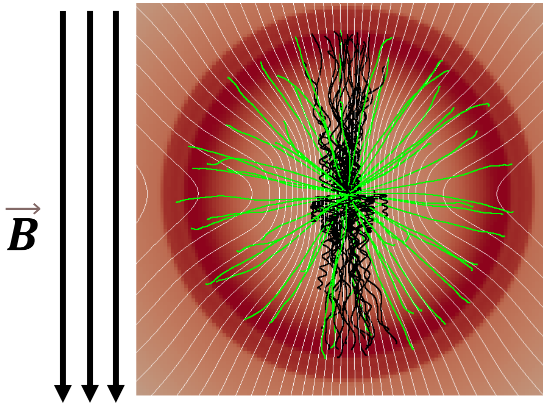

Magnetized *and* ***unmagnetized*** *α-particles trajectories over the hotspot of an ICF imploded target*

Magnetic field compression

Can seed B-fields of ~10 Tesla be amplified to ~10 kTesla ?

1) Soaking of seed B-field into the target

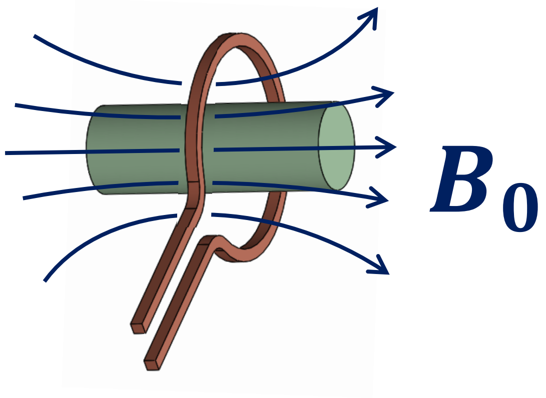

2) B-field amplified by advection with the imploding target

Laser beams for implosion

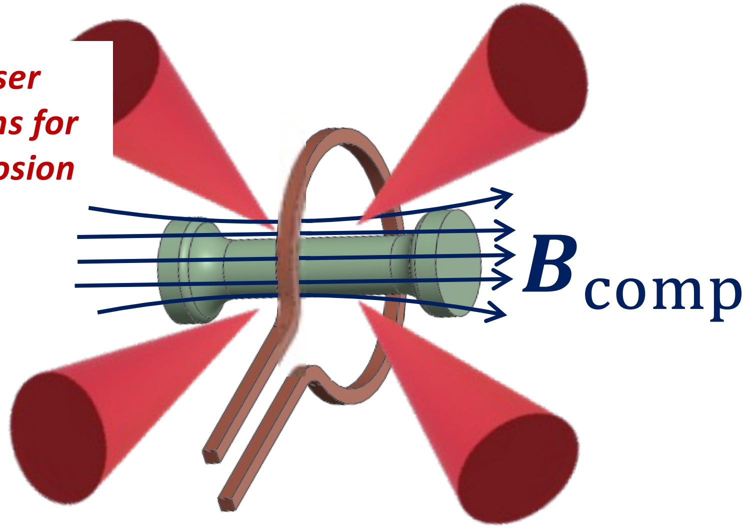

Resistive diffusion B-field advection

$$\frac{\partial \vec{B}}{\partial t} = -\vec{\nabla}\times\frac{\eta}{\mu_0}\vec{\nabla}\times\vec{B} + \vec{\nabla}\times\left(\vec{v}_B\times\vec{B}\right) + \cdots$$

Frozen-in-flow B-field compression

$$\frac{B_{\mathrm{comp}}}{B_0} = \left(\frac{R_0}{R}\right)^{2(1-1/R_m)} \xrightarrow[R_m \gg 1]{} \left(\frac{R_0}{R}\right)^2$$

Magnetic Reynolds number

$$R_m = \frac{\tau_d}{\tau_i}$$

Magnetic diffusion time $\tau_d = \mu_0 R_0^2/\eta$

Implosion time $\tau_i = R_0/v_{imp}$

***$B/B_0 \sim 500$, $BR \sim 0.04$ T.m** previously demonstrated at OMEGA with 15 kJ laser drive*

Hohenberger *et al.*, Phys. Plasmas **19**, 056306 (2012)

Magnetized implosions

Extended MHD

EUROfusion

Design and interpretation of the experiments rely on MHD codes including effects representing the transport of energy, currents and magnetic flux in a plasma

Resistive diffusion B-field advection Production of B-field by Biermann battery and ionization gradients

$$\frac{\partial \vec{B}}{\partial t} = -\vec{\nabla}\times \frac{\alpha_\parallel}{\mu_0 e^2 n_e^2}\vec{\nabla}\times\vec{B} + \vec{\nabla}\times(\vec{v}_B\times\vec{B}) + \vec{\nabla}\times\left(\frac{\vec{\nabla}p_e}{en_e} - \frac{\beta_\parallel\vec{\nabla}T_e}{e}\right)$$

B-field advection velocity :

$$\underline{v}_B = \underline{v} - \underbrace{\gamma_\perp \nabla T_e}_{\text{Nernst}} \underbrace{-\gamma_\wedge(\hat{\underline{b}}\times\nabla T_e)}_{\text{Cross-gradient-Nernst}} \underbrace{-\frac{\underline{j}}{en_e}(1+\delta_\perp^c)+\frac{\delta_\wedge^c}{en_e}(\underline{j}\times\hat{\underline{b}})}_{\text{Hall terms}}$$

Heat flux :

$$\underline{q}_\kappa = \underbrace{-\kappa_\parallel\nabla_\parallel T_e}_{\text{Conduction along B-field lines}} \underbrace{-\kappa_\perp\nabla_\perp T_e}_{\text{Suppressed conduction perpendicular to B}} - \underbrace{\kappa_\wedge \hat{\underline{b}}\times\nabla T_e}_{\text{Righi-Leduc heat flow}}$$

Extended-MHD 2D Gorgon simulations [1]

laser heating

- Ray-tracing
- Inverse bremsstrahlung

thermal transport

- Anisotropic conduction
- Righi-Leduc

radiation transport

- Non-diffusive multi-group approx.

magnetic transport

- **Advection:**
  - Bulk plasma
  - Nernst + cross-gradient Nernst
- **Source terms:**
  - Bierman Battery
  - Sadler
- **Resistive diffusion**

others

- Lorentz force
- Updated transport coefficients [2]

---

[1] Chittenden *et al.*, PPCF **46** B4567 (2004)
Walsh *et al.*, Phys. Rev. Lett. **118**, 155001 (2017)
Ciardi *et al.*, Phys. Plasmas **14**, 056501 (2007)

[2] Sadler *et al.*, Phys. Rev. Lett. **126**, 075001 (2021)

Magnetic-field-assisted spherical implosions at NIF

NIF scientists succeeded proof-of-principle experiment of magnetized indirect drive

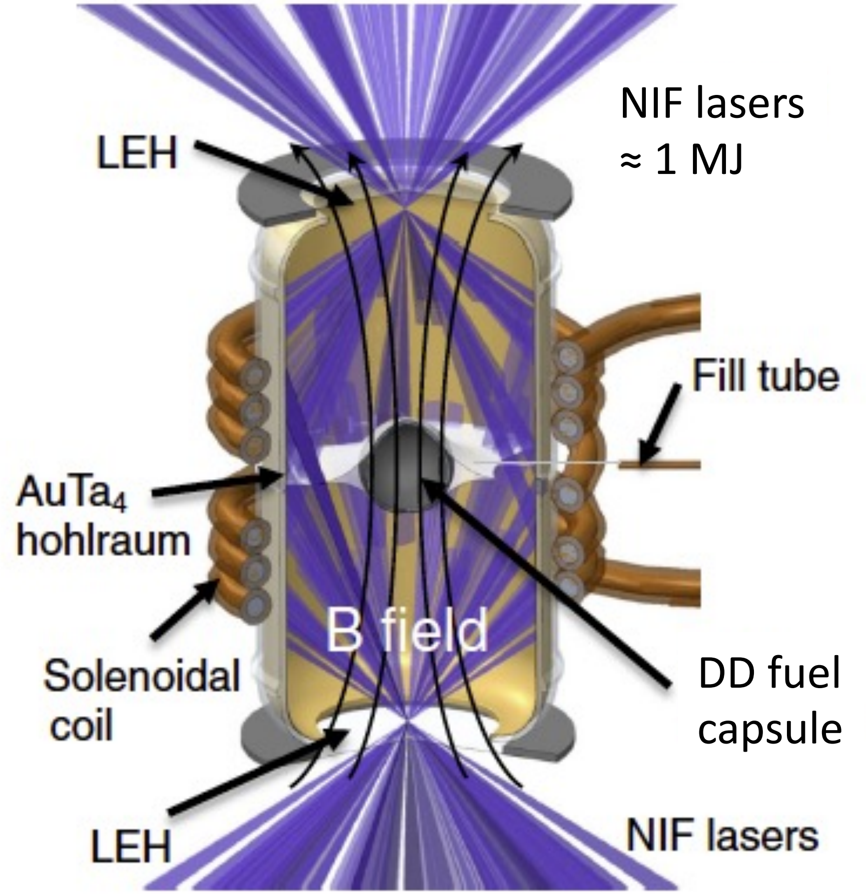

26 T seed B-field applied to a D_2-filled capsule indirectly driven at NIF:

- 40% increase ion temperature T_i
- 3.2x increase in neutron yield Y_{DD}

Moody *et al.*, Phys. Rev. Lett. **129**, 195002 (2022)

Spherical implosion experiments are inherently **asymmetric**, due to the applied B-field

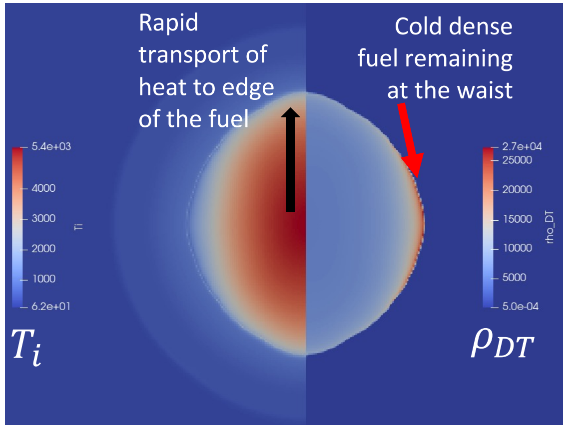

- Enhanced electron conduction along the pole
- Increased shock velocity at the waist due to reduced electron pre-heat

Cylindrical geometry ideally suited to interrogate MHD models

Novel cylindrical implosion platform at the OMEGA-60 laser facility with dopant K-shell emission spectroscopy to infer plasma conditions of the core

Cylindric plastic shells filled with D_2 at 11 atm with 0.13% atomic concentration of Ar doping for spectroscopic tracing

$\vec{B}$ parallel to cylinder axis and target compressed radially

CH shell

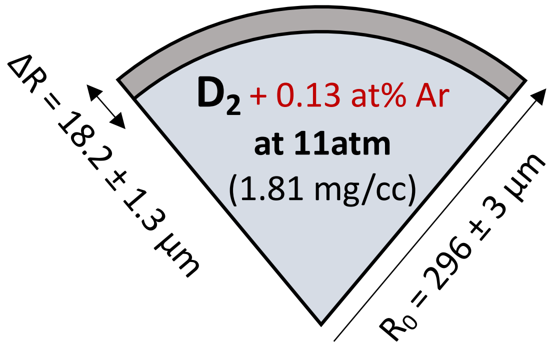

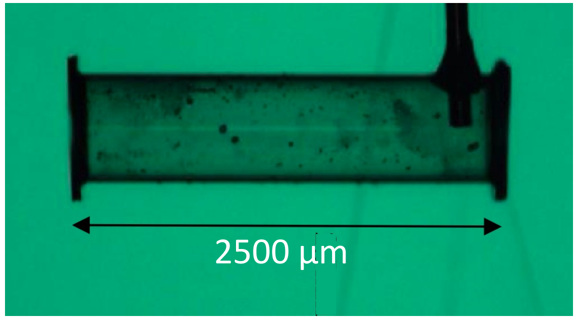

Seed B-field of B_0 = 30 T driven externally by a capacitor bank discharge (~µs pulses)

MIFEDS: Gotchev *et al.* Rev. Sci. Inst. **80**, 043504 (2009)

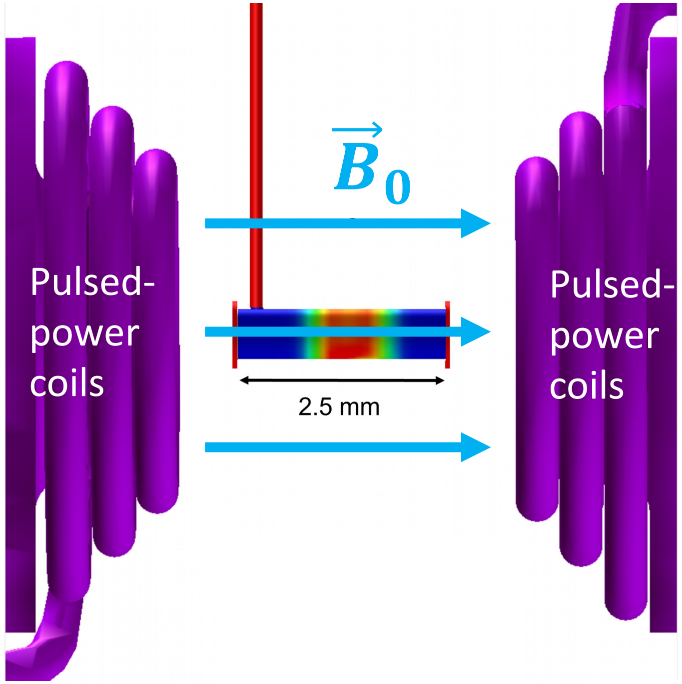

Laser drive: 40 UV beams, 1.5 ns, total energy of 14.5 kJ

> 5×10^{14} W/cm^2 fairly uniform across 650 µm

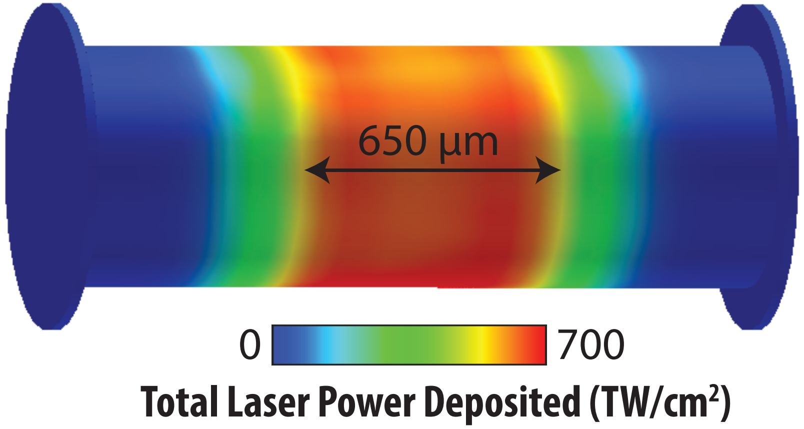

Walsh *et al.*, Plasma Phys. Control. Fusion **64**, 025007 (2022)
Bailly-Grandvaux *et al.*, Phys. Rev. Research **6**, L012018 (2024)

Magnetized cylindrical implosions at OMEGA

Core conditions strongly modified by the compressed B-field

Predictions from 2D extended-MHD simulations

***Evolution of the** mass-averaged*
core plasma conditions

Magnetized implosion (B_0 = 30 T)

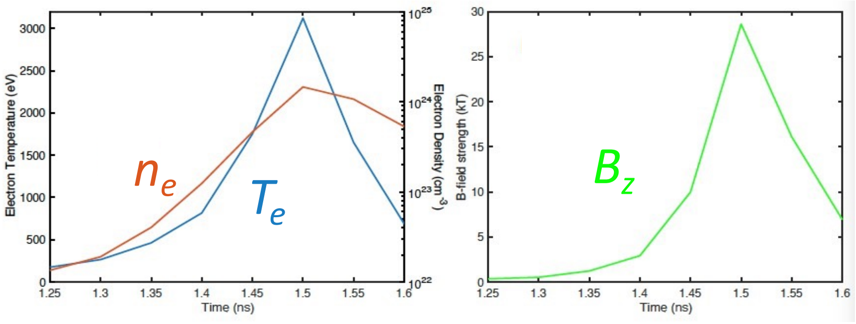

Unmagnetized implosion (B_0 = 0)

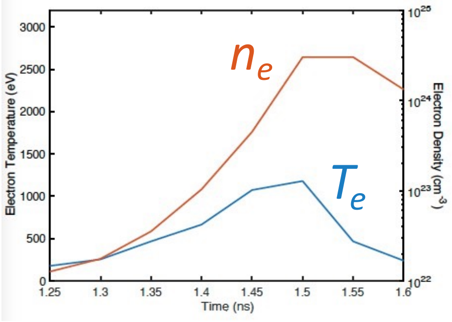

Plasma conditions at t = 1.45 ns
($B_z \sim 10$ kT)

Electron temperature ***Mass density***

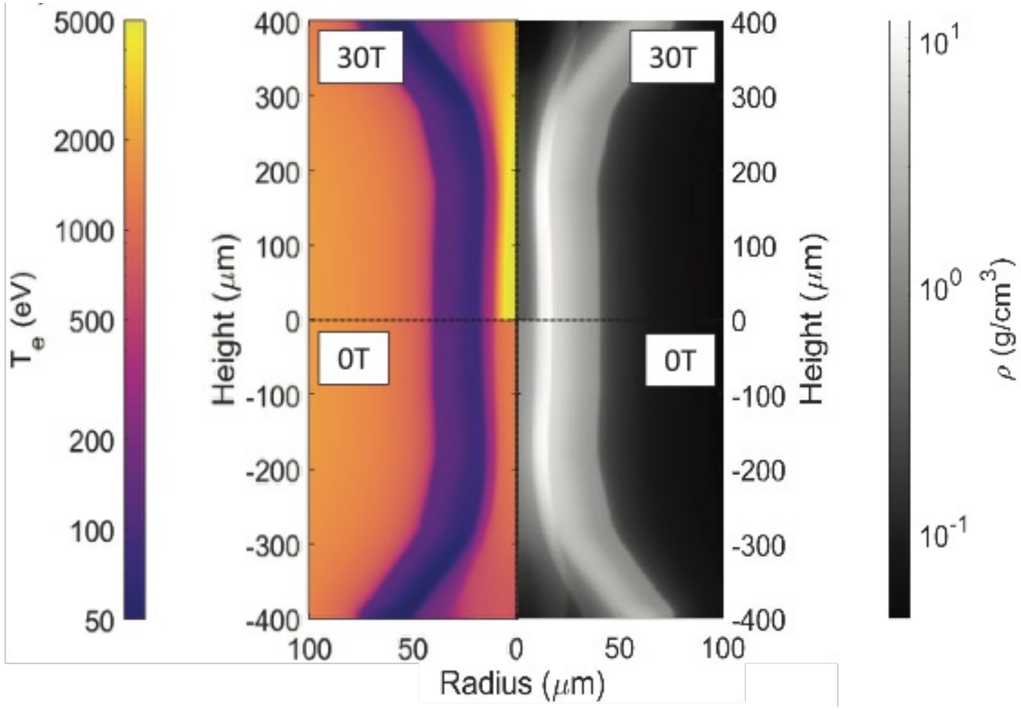

When applying B_0 = 30 T, the resulting compressed core is

- **hotter** because **highly magnetized**
- **less dense** as it hosts a **large magnetic pressure**

Walsh *et al.*, Plasma Phys. Control. Fusion **64**, 025007 (2022)

Magnetized cylindrical implosions at OMEGA

Implosion reaching a compression ratio $CR \sim 20$

X-ray pinhole imaging framing cameras with two orthogonal views

Experimental data

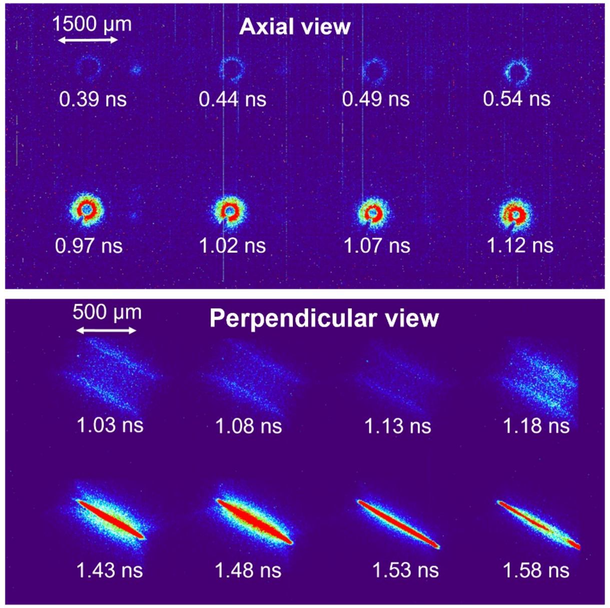

Synthetic images :

MHD + Radiation transport + Instrum. Resp.

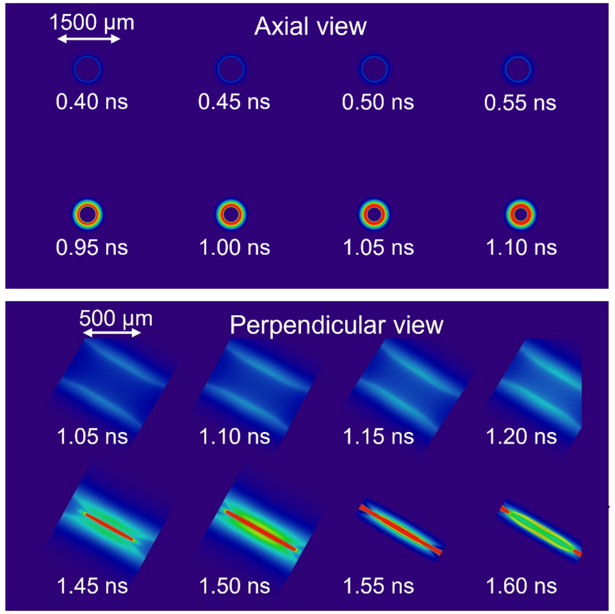

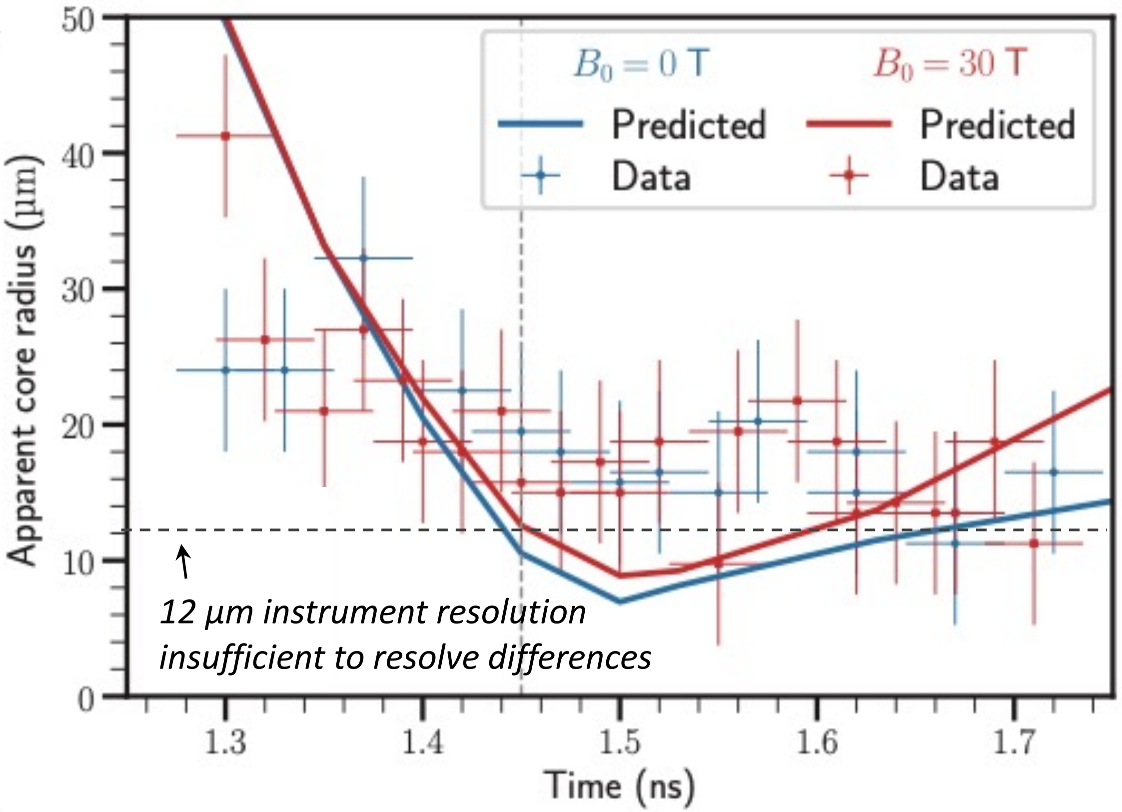

12 µm instrument resolution insufficient to resolve differences

Apparent similar compression with and w/o B-field, despite the different plasma conditions

Differences *between $B_0 = 0$ T and $B_0 = 30$ T, predicted by MHD simulations,* ***indiscernible due to resolution limit***

Fuel compression reduced vs MHD predictions

Measured convergence ratio of $CR = R_0/R_f \sim 20$ (vs $CR \sim 40$ in MHD sims)

Pérez-Callejo *et al.*, Rev. Sci. Instrum. **93**, 113542 (2022)
Bailly-Grandvaux *et al.*, Phys. Rev. Research **6**, L012018 (2024)

Hotter magnetized plasma evidenced by spectral changes

Observed a total of 6 main Ar K-shell emission lines in two different charge states of Ar

Experimental time-integrated argon K-shell emission

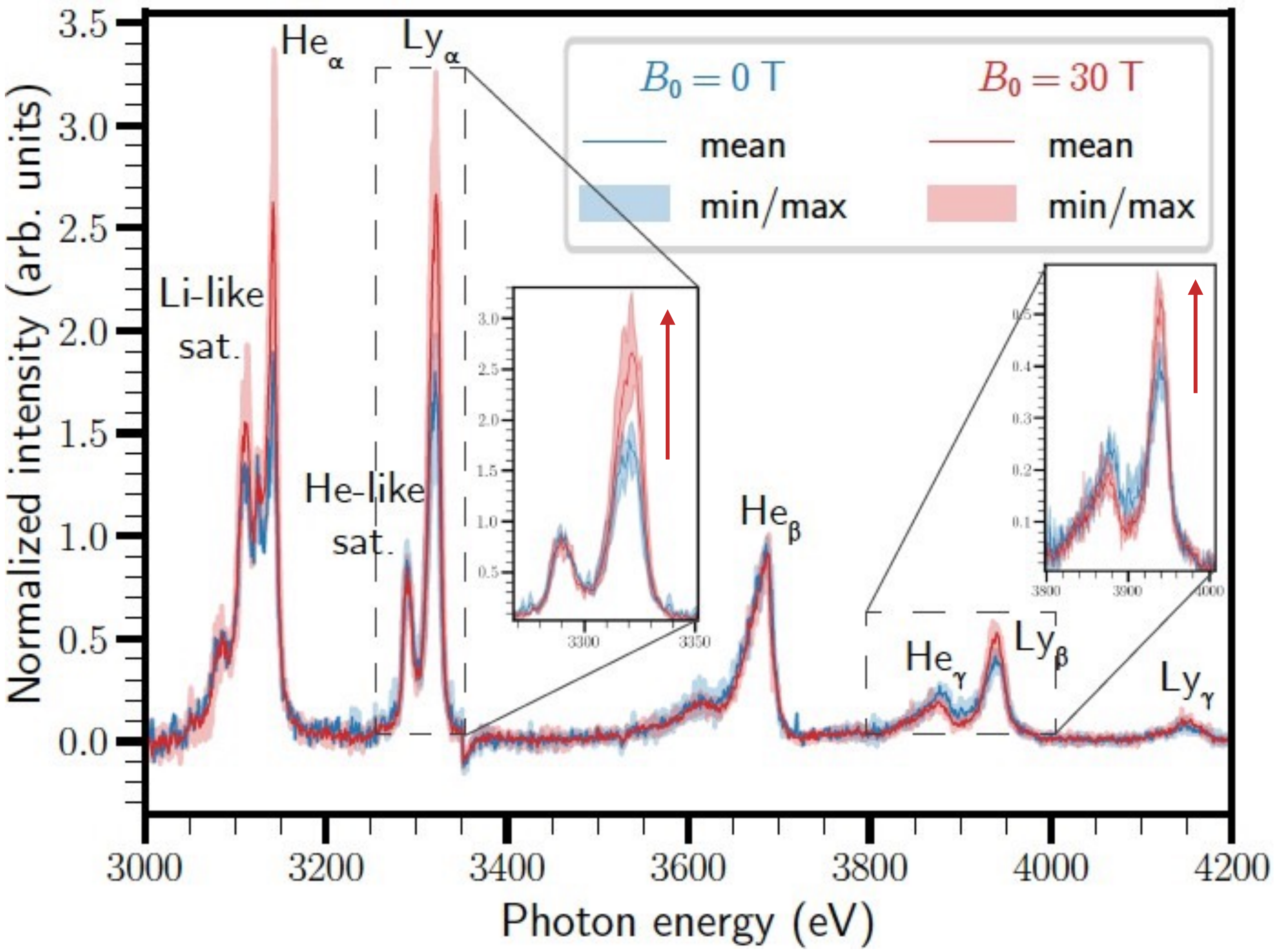

Reproducible spectra for both **magnetized** and **unmagnetized** cases

(over 6 shots : 4 with B-field, 2 w/o B-field)

Observed systematic changes between $B_0 = 30$ **T** and $B_0 = 0$ **T** :

Higher $\mathbf{Ly_\beta / He_\gamma}$ *and* $\mathbf{Ly_\alpha}$ ***/ He-like satellite line intensity ratios for the magnetized case***

H-like population increases in magnetized case

⇒ **Evidence of a hotter core**

Bailly-Grandvaux *et al.*, Phys. Rev. Research **6**, L012018 (2024)

Magnetized cylindrical implosions at OMEGA

Post-processed MHD sims agree with experimental spectra

EUROfusion

Time-integrated ***experimental data* vs. *synthetic spectra*** *(from post-processing of MHD simulations)*

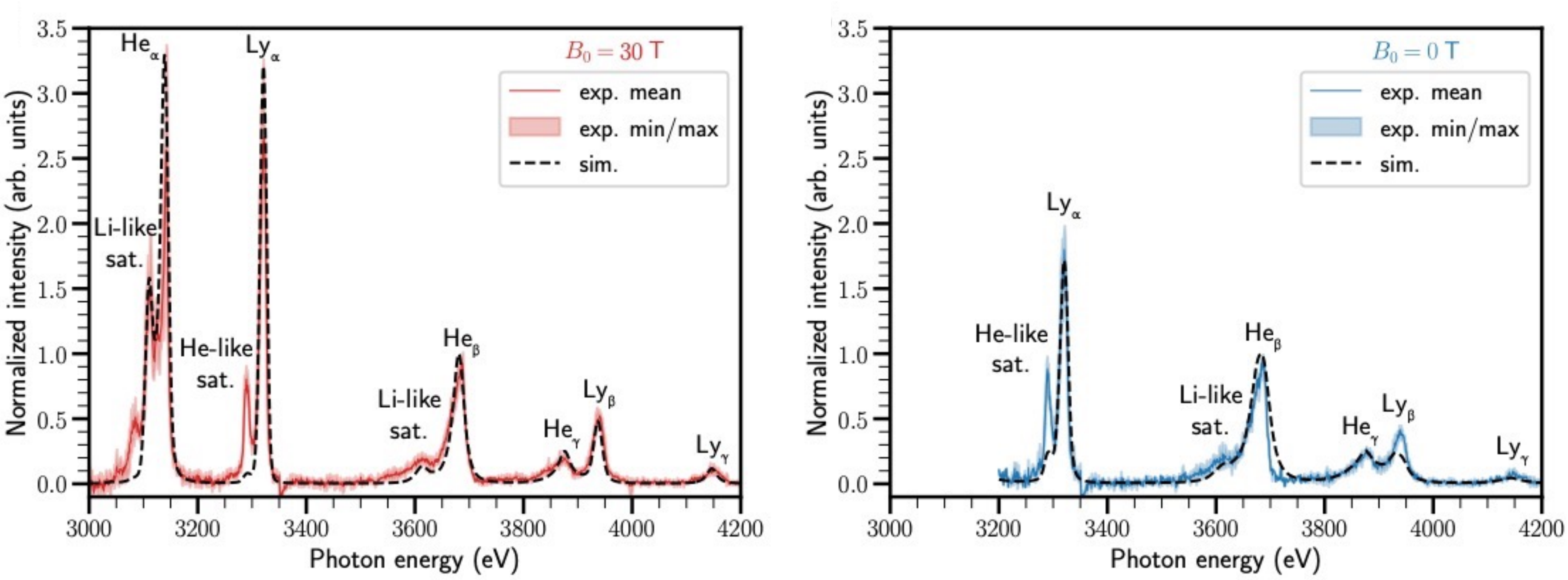

Match between synthetic and experimental spectra allows to extract the **compressed B-field at the time of experimental peak compression**

$$\boldsymbol{B}_{\mathbf{comp}} \sim \mathbf{10\ kT},$$

$$BR \sim 0.1\ \mathrm{T.m} \quad \text{at} \quad CR \sim 20$$

Bailly-Grandvaux *et al.*, Phys. Rev. Research **6**, L012018 (2024)

Spectroscopy analysis independent of MHD input

Experimental relative intensities and Stark- and opacity-broadened line profiles satisfactorily reproduced

(up to 6 primary line transitions spanning in two different charge states), for both magnetized and unmagnetized cases

Spectral calculations consider the whole apparatus of **non-LTE atomic kinetics**[1], **Stark-broadening theory**[2] and **radiation transport**

[1] Florido *et al.*, Phys. Rev. **E** 80, 056402 (2009)

[2] Mancini *et al.*, Comput. Phys. Commun. **63**, 314 (1991)
Ferri *et al.*, Matter Rad. Extremes **7**, 015901 (2022)
Gigosos et al., Atoms **9**, 9 (2021)

Combination of multi-zone (6) spectroscopic model with random-search χ2-minimization:

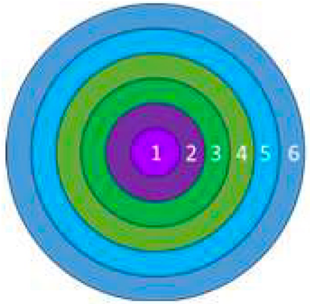

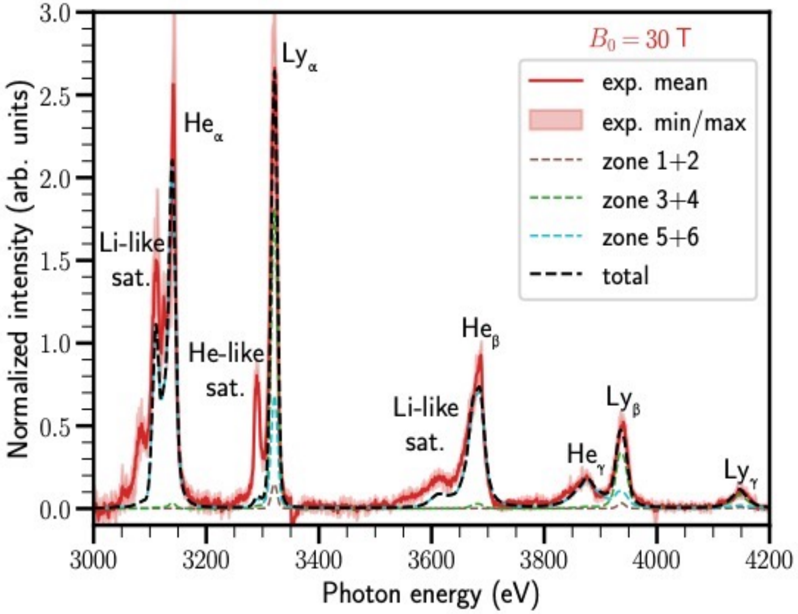

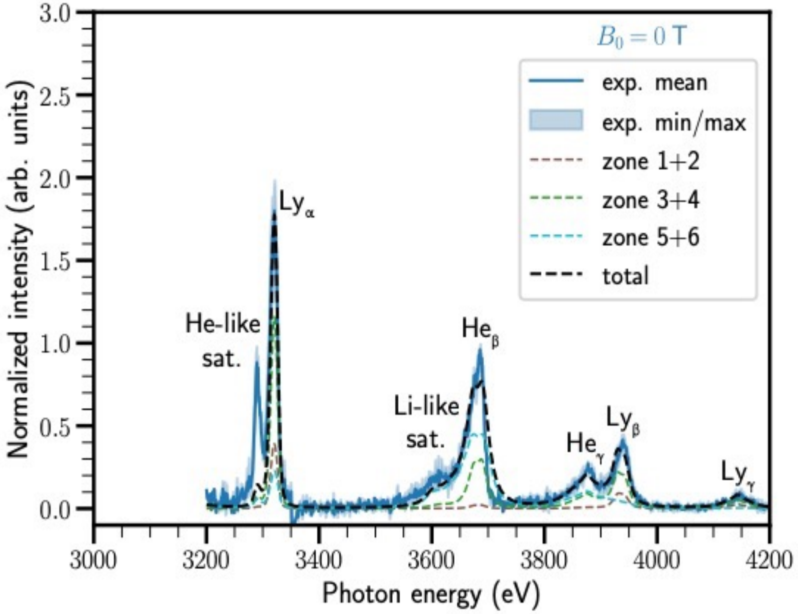

$$T_e^{30T} = 1476 \pm 127 \text{ eV}$$

$$\rho^{30T} = 1.49 \pm 0.11 \text{ g/cm}^3$$

$$T_e^{0T} = 1000 \pm 30 \text{ eV}$$

$$\rho^{0T} = 3.22 \pm 0.16 \text{ g/cm}^3$$

Analysis converge to a core temperature increase by ~ 50% and core density decrease by a factor ~ 2, in line with findings from the MHD simulations

The cylindrical implosions are affected by a strong magnetization $(\omega_{ce}\tau_{ei} \sim 85)$ **and significant magnetic pressure** $(\beta \sim 7)$

Bailly-Grandvaux *et al.*, Phys. Rev. Research **6**, L012018 (2024)

Magnetized cylindrical implosions at NIF

Moving the platform to ignition scale facilities

Magnetized cylindrical implosion experiments offer insights into the physics of heat and magnetic flux transport

***Discovery Science* project granted at NIF** (2 shot days in 2024 and 2025)

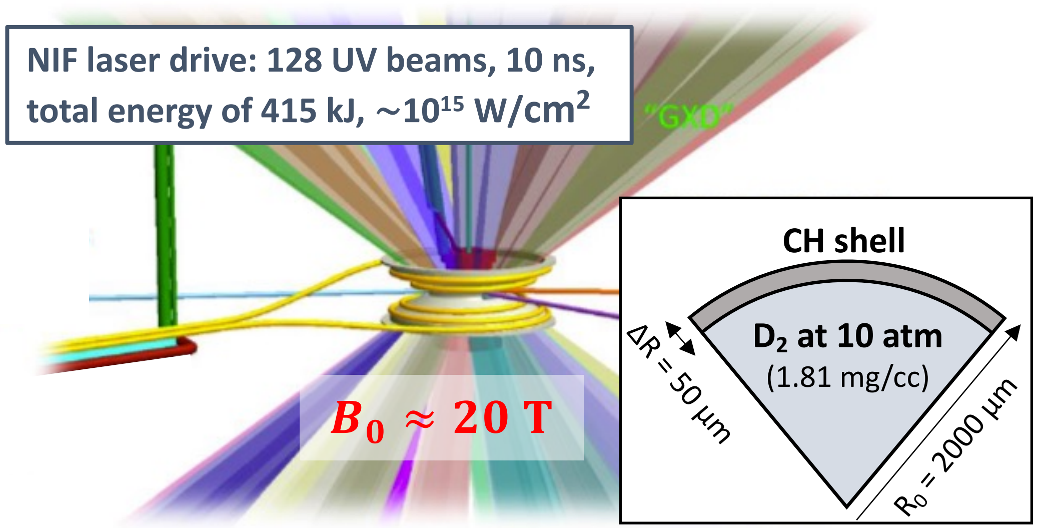
NIF laser drive: 128 UV beams, 10 ns, total energy of 415 kJ, ~10^{15} W/cm^2

$B_0 \approx 20$ T

- **25x more laser energy** and **6x larger targets** than at OMEGA
- Predicted formation of a 50-100 µm radius core, with ***BR up to 0.9 Tm*** *(~0.1 Tm at OMEGA)*

⇒ **Enables tritium trapping**

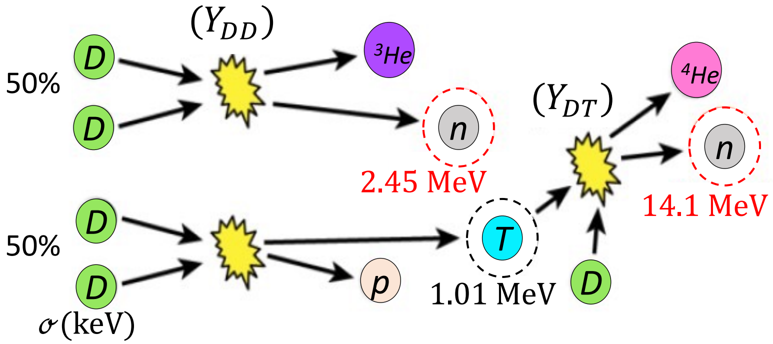

Compressed magnetic field strength and **topology** can be characterized from angularly resolved ToF spectra of secondary neutrons

Schmitt *et al.*, Phys. Rev. Lett. **113**, 155004 (2014)

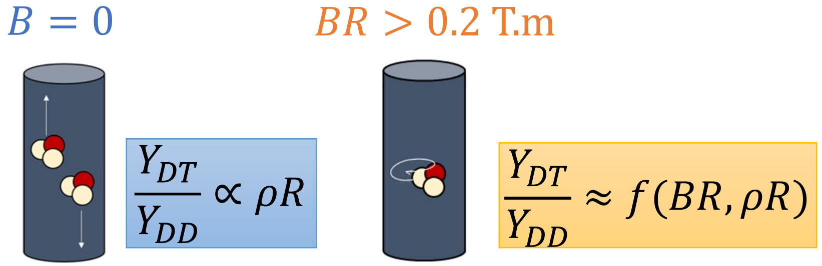
$B = 0$

$\frac{Y_{DT}}{Y_{DD}} \propto \rho R$

$BR > 0.2$ T.m

$\frac{Y_{DT}}{Y_{DD}} \approx f(BR, \rho R)$

Magnetized cylindrical implosions at NIF

First experimental results obtained in June 2024

EUROfusion

X-ray imaging and streaked Ar K-shell emission suggest a maximum compression ratio CR ~ 13 at 9-10 ns time (MHD simulation predicted $CR \sim 20$ at 11 ns)

Implosion dynamics inspected from 50 ps-gated X-ray images

$$v_{imp} \approx 12\ \mathrm{km/s}$$

Magnetized shot, B_0 = 16.5 T

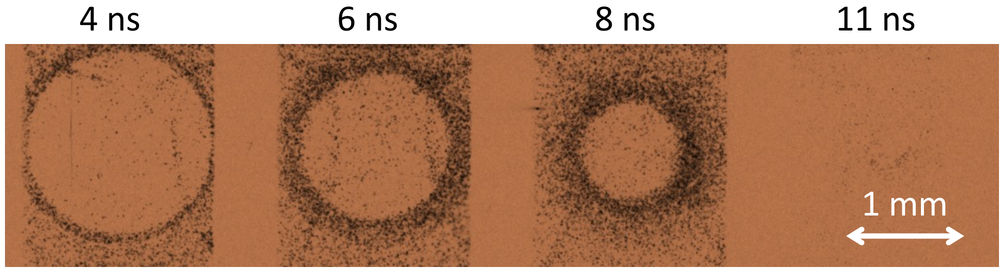

Unmagnetized shot

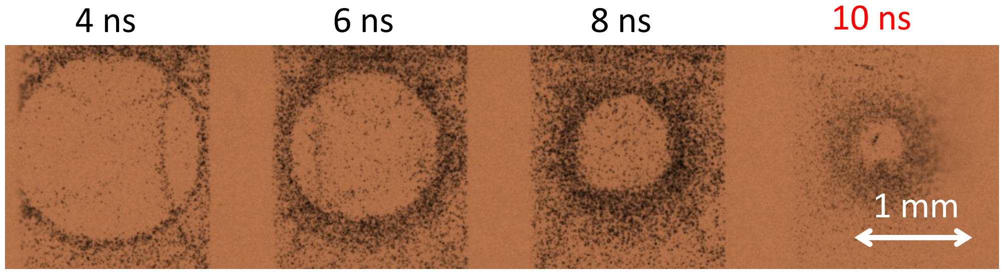

Suspected target dismantlement due to RT instability

Time-resolved Ar K-shell emission spectra

Magnetized shot, B_0 = 16.5 T

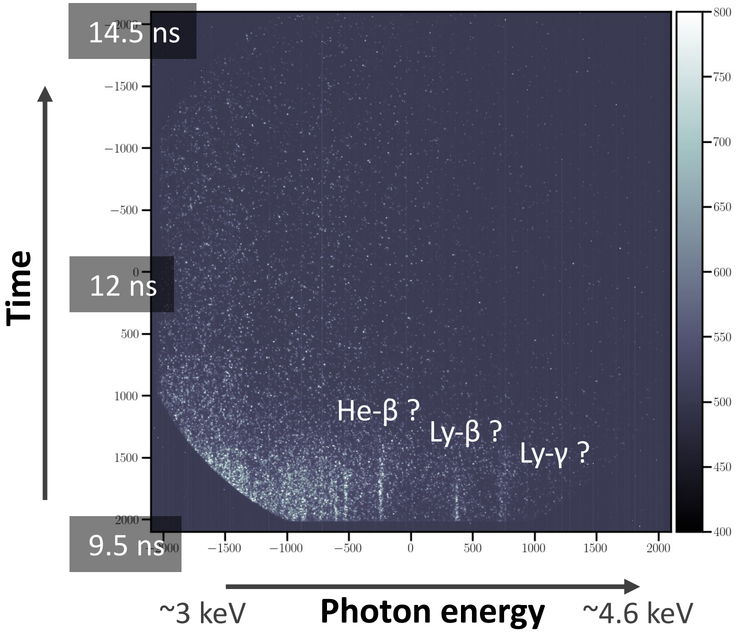

Unmagnetized shot

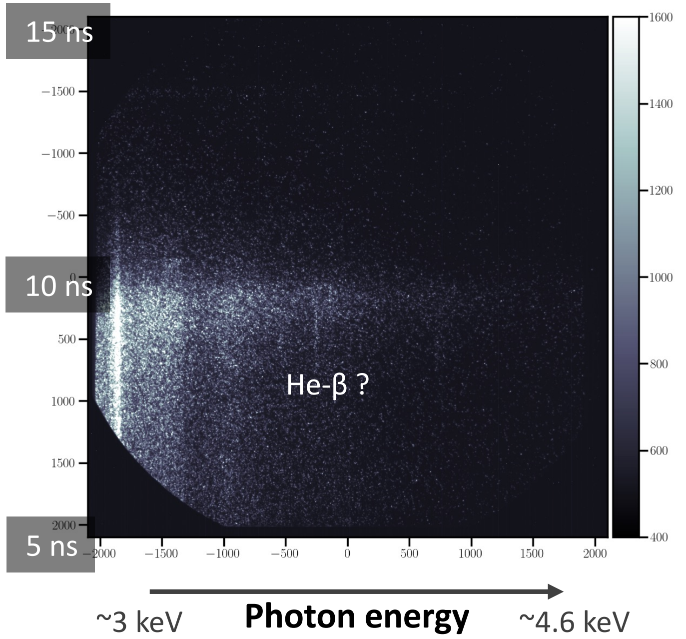

Ar K-shell lines observed when external B-field is applied, but their identification is difficult

Magnetized cylindrical implosions at NIF

The imposed B-field seems to help stabilizing the implosion

X-ray imaging and streaked Ar K-shell emission suggest a maximum compression ratio CR ~ 13 at 9-10 ns time
(MHD simulation predicted *CR* ~ 20 at 11 ns)

Implosion dynamics inspected from 50 ps-gated X-ray images

$v_{imp} \approx 12\ \mathrm{km/s}$

Magnetized shot, B_0 = 16.5 T

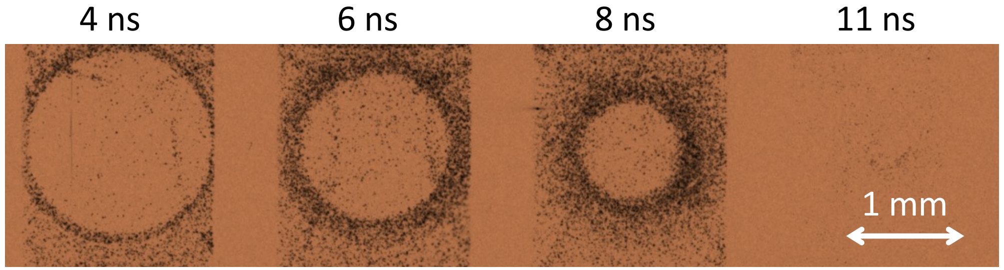

Unmagnetized shot

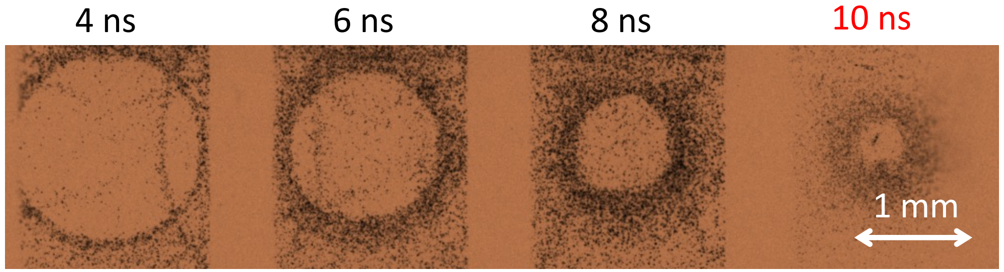

Magnetized shot
B_0 = 16.5 T

Unmagnetized shot

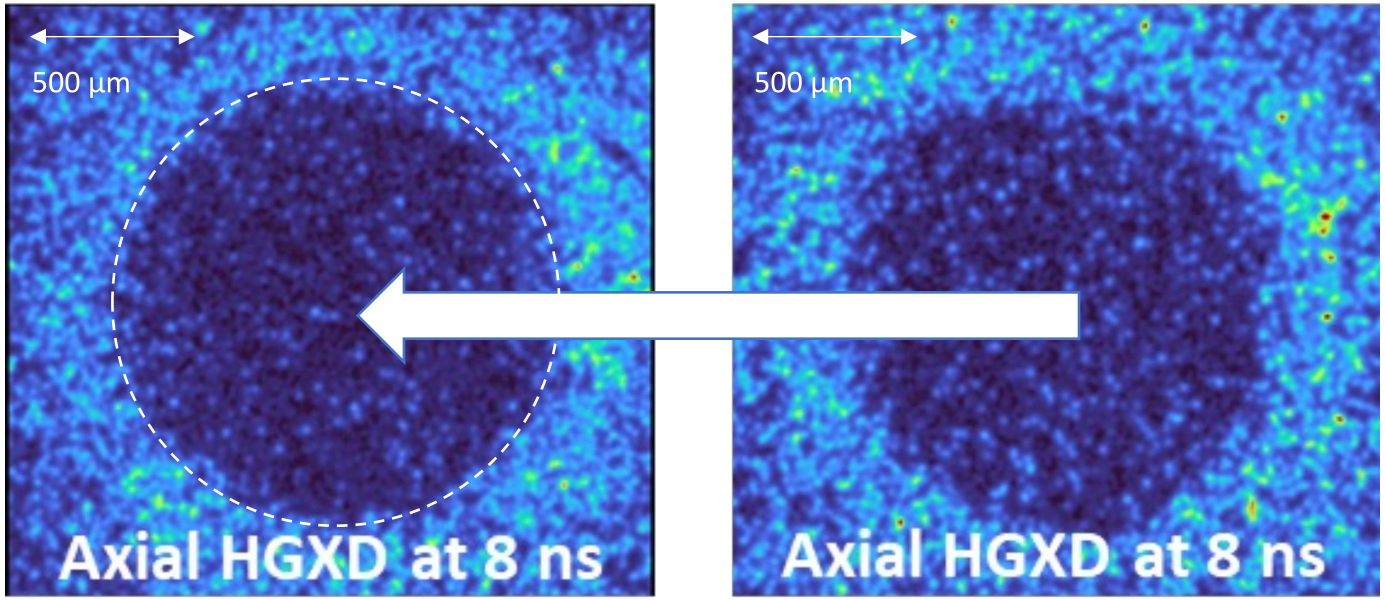

A more uniform implosion with applied B-field

Magnetized cylindrical implosions at NIF

The magnetized shot has about 3x higher DD neutron yield

ToF signals from primary DD-fusion neutrons

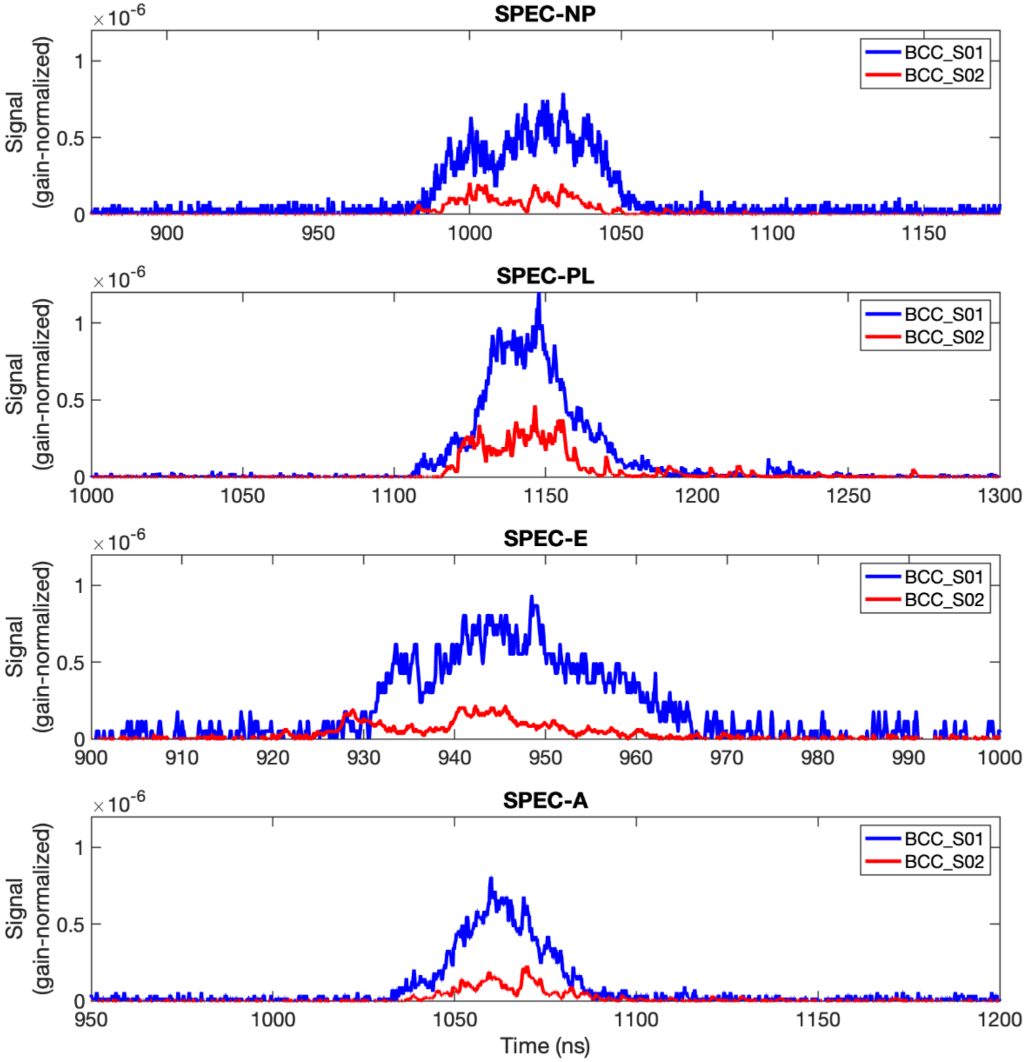

	θ	ϕ
NP	18°	303°
PL	63°	70°
E	90°	174°
A	116°	316°

Increase ($\sim 3\times$) **in primary neutron yield for magnetized shot in all 5 ToF detectors,** but…

- $Y_{DD}^{n} \sim 10^9$ (vs. 10^{11} expected)
- No DT neutrons detected

Increase in neutron yield likely originates from the more stable implosion with applied B-field

Magnetized cylindrical implosions at NIF

Ar emission in the magnetized case indicates $\sim$1.4 keV core $\langle T_e \rangle$

Time-integrated Ar K-shell spectrum

NXS raw Image Plate images

Unmagnetized shot

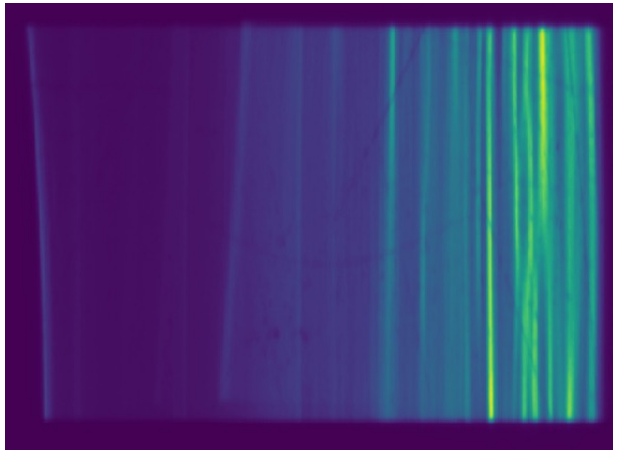

Magnetized shot

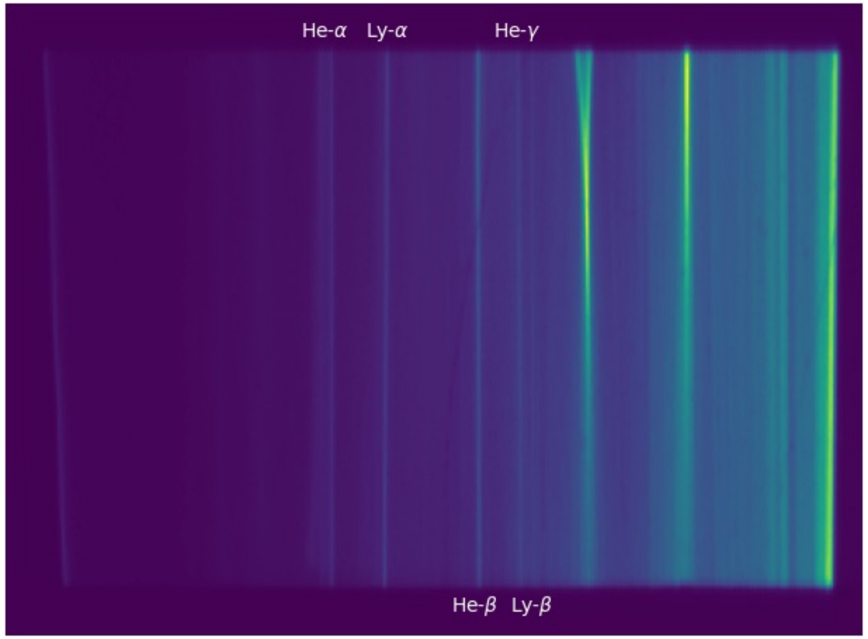

Magnetized shot spectra:
Lineout from time-integrated data
vs. 2-zones spectroscopic model

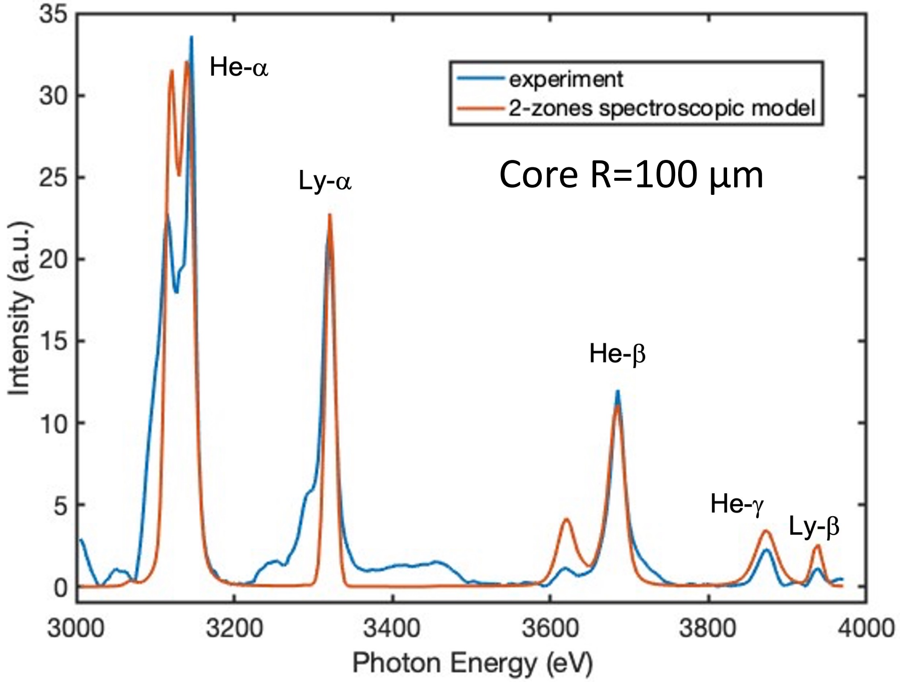

With external B-field applied, the average core temperature is estimated to be ~ 1.4 keV (~ 2 keV expected)

In the unmagnetized shot, crystal defects are obscuring the Ar line emission

Recent extended-MHD simulations show instabilities

2D CHIMERA simulations

10 ns drive, 3 kJ/beam

4 mm initial OD

including 3D ray tracing

Snapshots close to stagnation (t=9.6 ns)

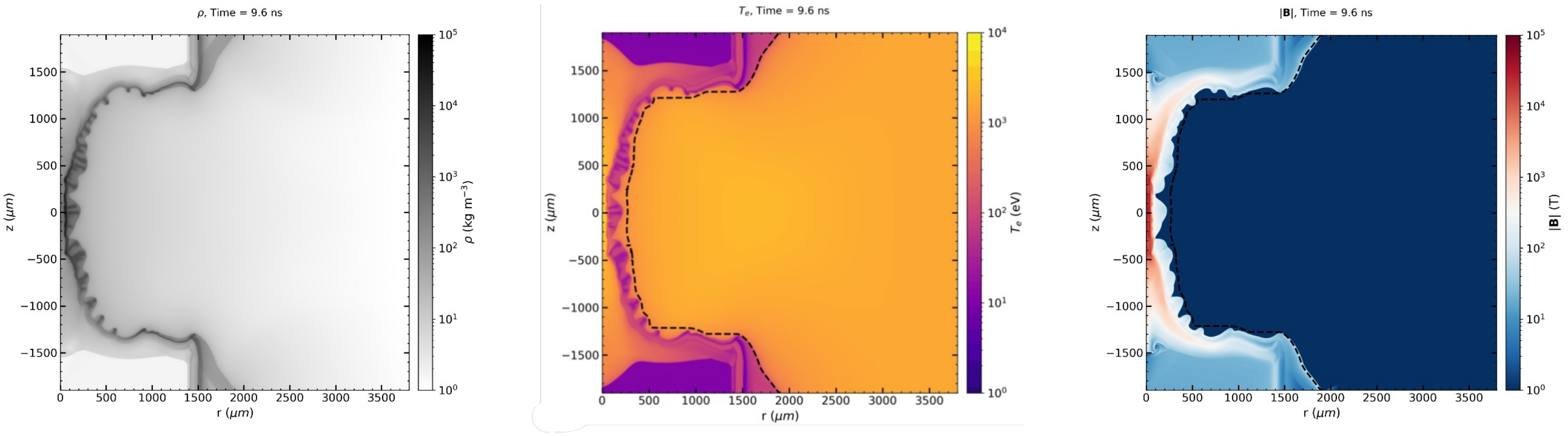

Density

Electron temperature

B-field

Magnetized cylindrical implosions at NIF

We aim to stabilize the implosions on the upcoming 2025 shots

Increase stability with thicker shell (50 µm → 100 µm) and higher fuel mass (10 atm → 20 atm)

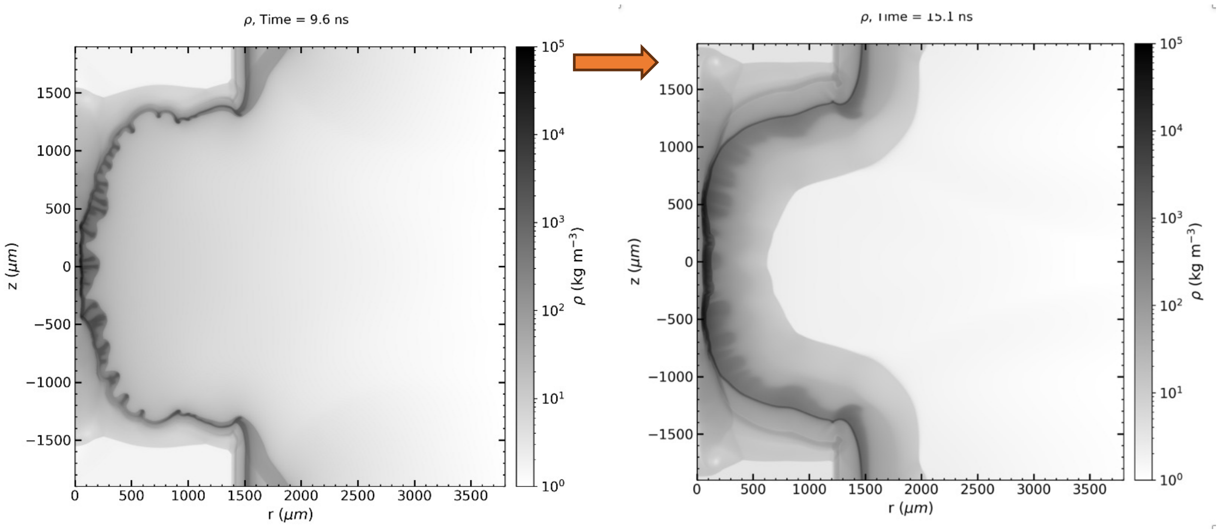

The thicker shell should be less prone to instabilities and shredding

- Bang time is reached later, at ∼15 ns
- DD yield is reduced from 10^{11} to $4\mathrm{x}10^9$

Optimizing the pulse-shape (flat top → custom pulse shape)

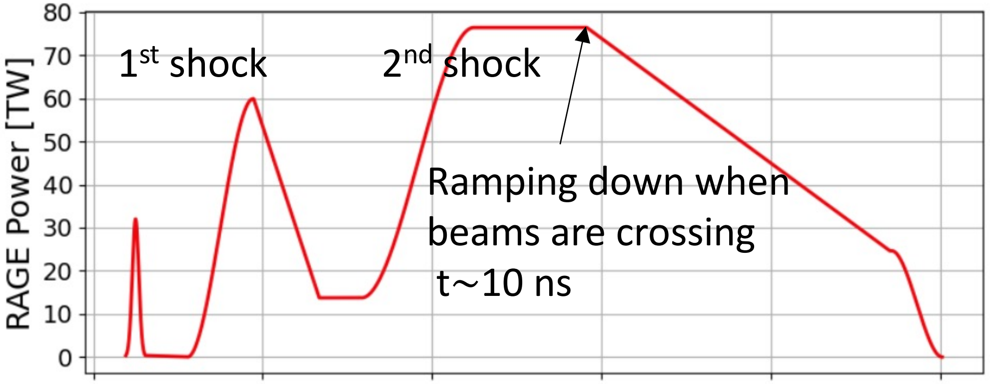

Optimization runs ongoing performed with xRAGE code to increase yield while maintaining a stable implosion

Magnetized cylindrical implosions at LMJ

Moving the platform to ignition scale facilities

Magnetized cylindrical implosion experiments offer insights into the physics of heat and magnetic flux transport

***LMJ shots** granted through Association Laser-Plasma*
re-scheduled to 2027

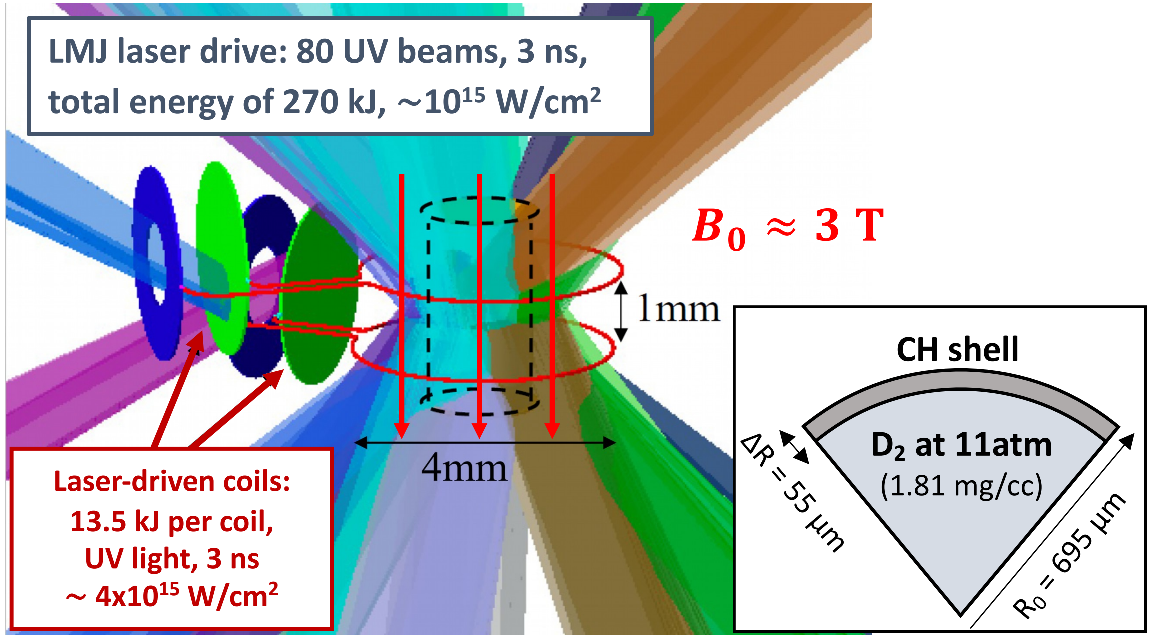

LMJ laser drive: 80 UV beams, 3 ns, total energy of 270 kJ, ~10^{15} W/cm²

Laser-driven coils:
13.5 kJ per coil,
UV light, 3 ns
~ 4×10^{15} W/cm²

- **Drive energy comparable to NIF**
- Relatively small targets (only 2x larger than at OMEGA) yield **very high compression, $CR \sim 60$**
- Constrained to $B_0 \sim 3$ T using laser driven-coils

4 kA discharges in 2000 µm-radius coils (already validated at LMJ)

⇒ 3 T seed B-field amplified to 10 kT from expected CR~60

Dual dopant (Ar + Kr) spectroscopy to **characterize core electron temperature with an effective spatial resolution**

Pérez-Callejo *et al.*, Phys. Rev. E **106**, 035206 (2022)

Magnetized cylindrical implosions at LMJ

Dual-dopant (Ar+Kr) spectroscopy "sees" into the magnetized core

EUROfusion

Large range of temperatures in the magnetized core, up to >2.5 keV, requires **addition of Kr-doping** to probe hottest regions

Predicted temperature profiles
for the stagnated plasma (t = 3.5 ns)

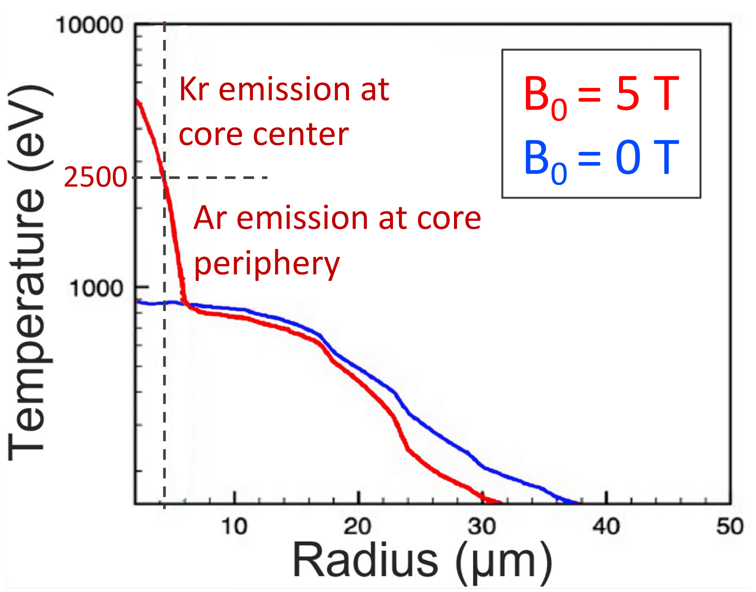

Predicted K-shell line emission spectra

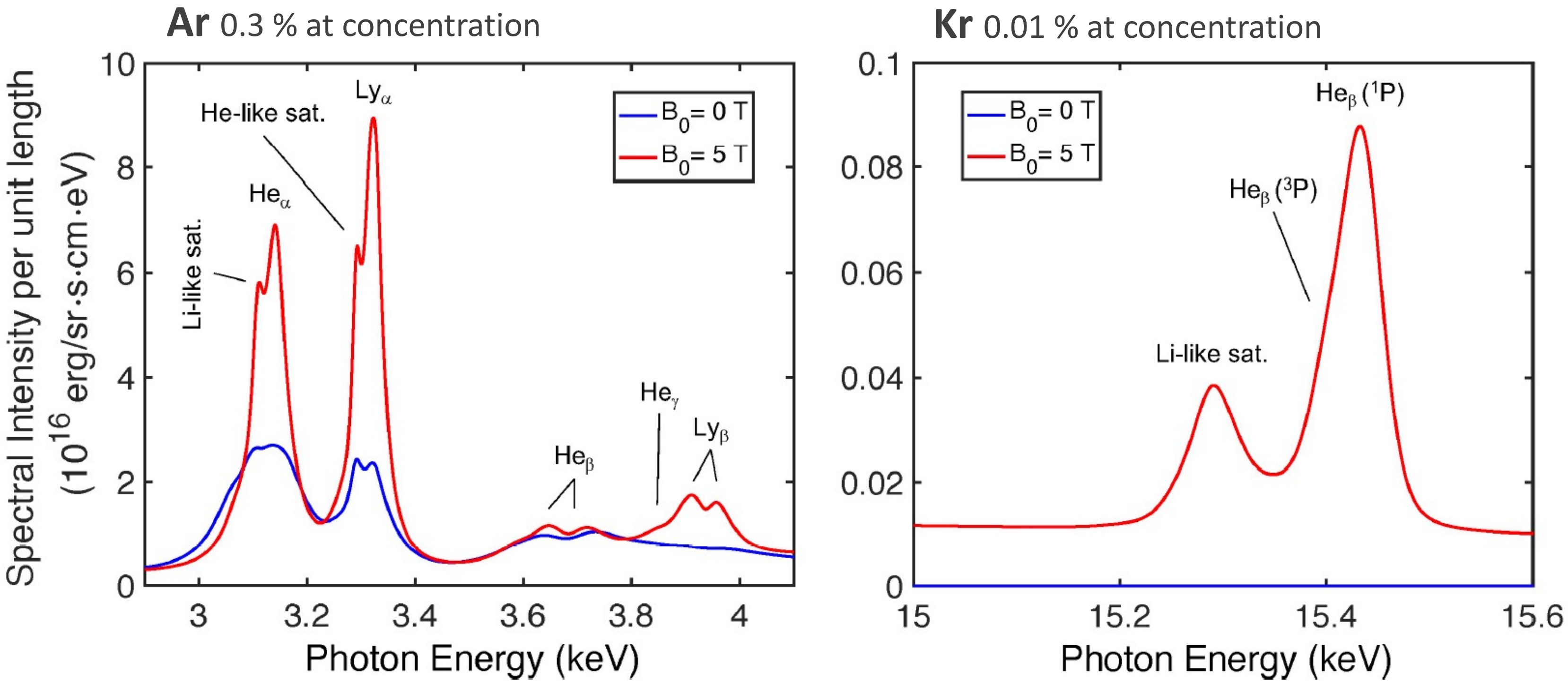

Large spectral differences predicted between unmagnetized and magnetized shots

In the magnetized core, the **dual-dopant** technique scrutinizes the magnetization effects at the **core periphery** (Ar emission for $T_e < 2.5$ keV) and at the **core center** (Kr emission for $T_e > 2.5$ keV)

⇒ **effective spatial resolution $T_e(r)$**

Pérez-Callejo *et al.*, Phys. Rev. E **106**, 035206 (2022)

Working principle for B-field generation in a laser-driven coil

RL-circuit fed by a laser-driven diode (current source)

Tikhonchuk *et al.*, Phys. Rev. E **96**, 023202 (2017)
Tikhonchuk, Santos, Korneev, ECLIM 2018
Williams *et al.*, J. App. Phys. **127**, 083302 (2020)

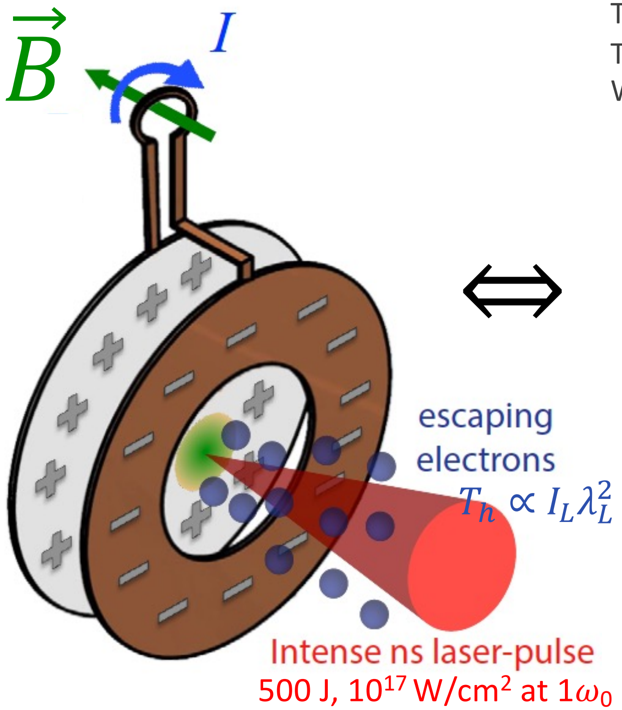

Intense ns laser-pulse
500 J, 10^{17} W/cm^2 at $1\omega_0$

$\Leftrightarrow$

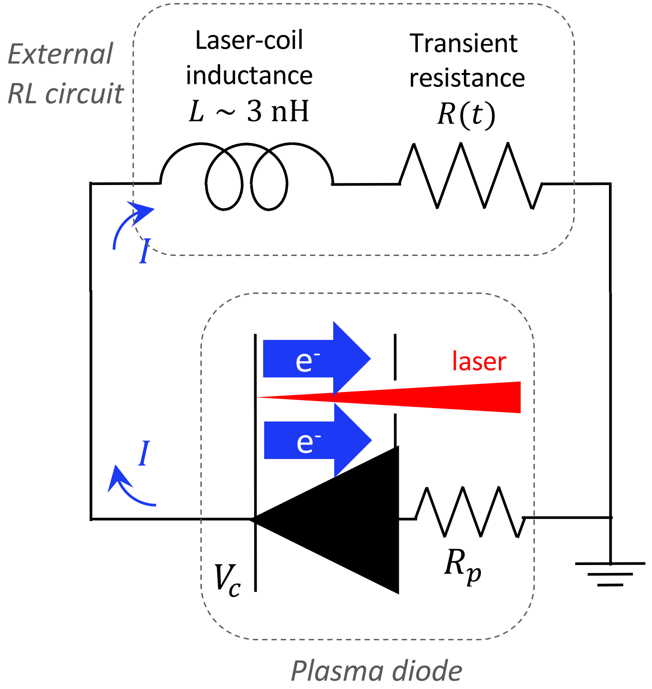

At the coil centre :

200 kA

$$B_0 \sim \frac{\mu_0 I}{2a} \approx 480\ T$$

coil radius
= 250 µm

$$\boxed{V_c - R_p I = L\frac{dI}{dt} + R(t)I}$$

Current-voltage characteristic

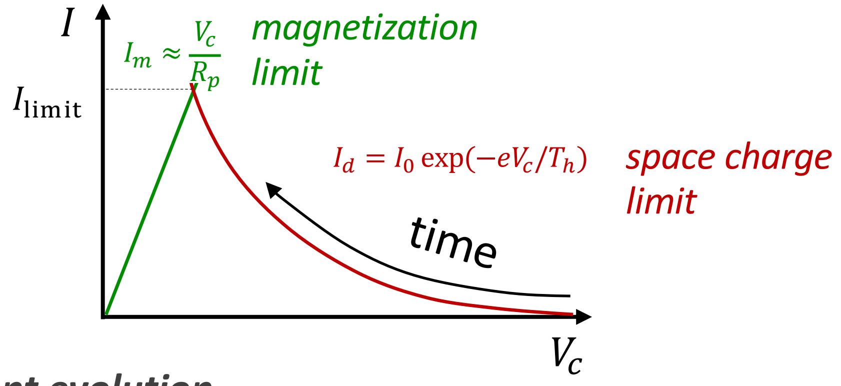

Current evolution

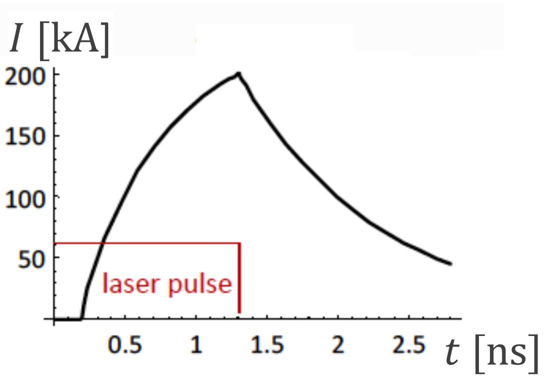

Raising time:

$$\tau_1 \sim I_{\rm max} L/V_c$$

Decay time:

$$\tau_2 \sim \frac{L}{R+R_p} \sim \frac{L}{R}$$

Key parameters controlling the peak current :

- Hot electron temperature $T_h \propto I_L \lambda_L^2$
- Impedance of the external circuit

Key parameters controlling the B-field duration :

- Laser pulse length
- Target inductance L

Laser-driven B-fields for magnetized HED experiments

LDC performance in different laser facilities

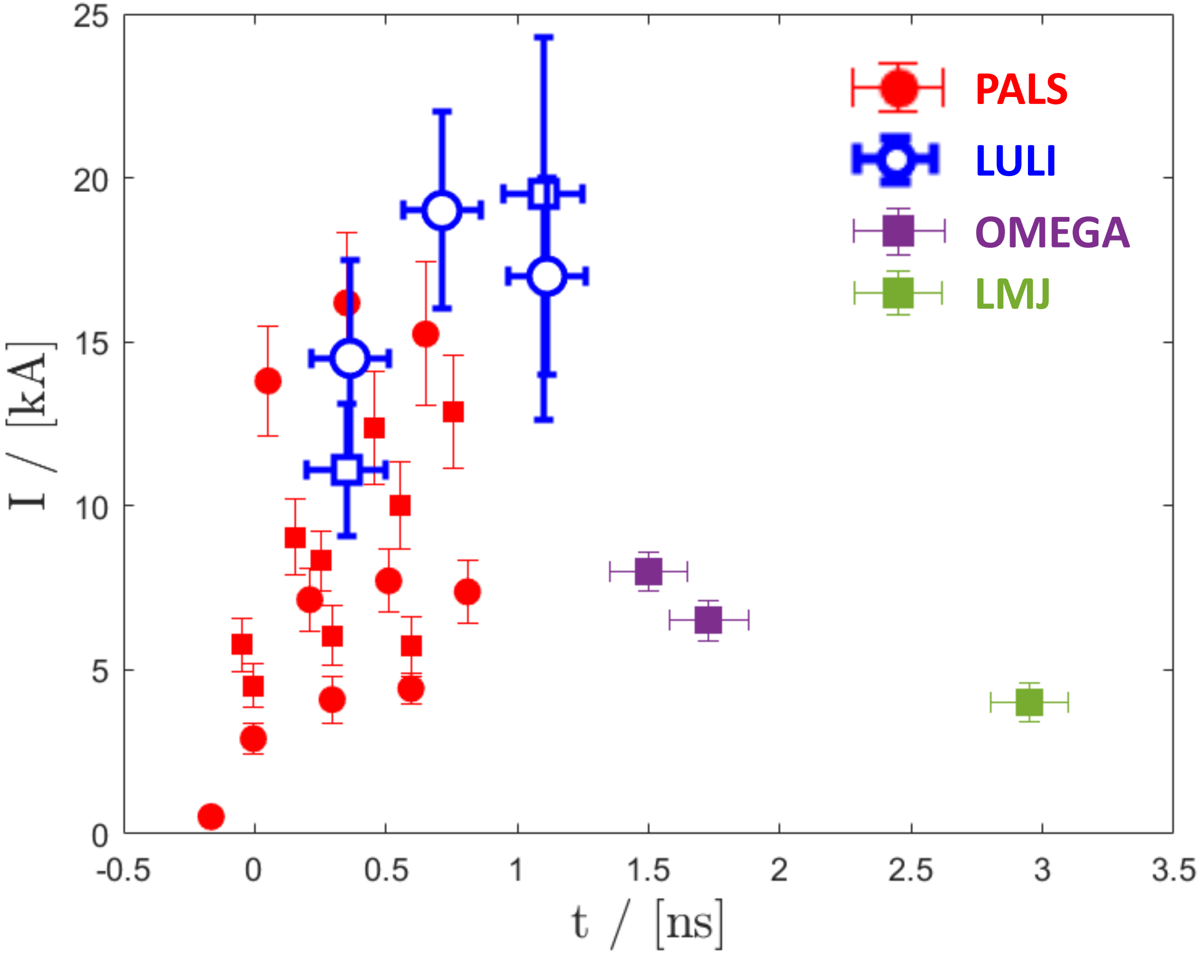

Important Parameters

For all cases intensity ranges
$10^{15} \leq I_{las} \leq 10^{16}$ W/cm²

@ PALS : E_{las}= 0.6 kJ, λ = 1.315 µm, L = 7 nH

@ LULI : E_{las}= 0.5 kJ, λ = 1.053 µm, L = 3.7 nH

@ OMEGA : E_{las}= 2 kJ, λ = 0.351 µm, L = 6.5 nH

@ LMJ: E_{las}= 12.5 kJ, λ = 0.351 µm, L = 7.9 nH

Lower peak B-fields are achieved in large scale facilities where large magnetized volumes are required

The lower wavelength (3ω) is not helping

ENR-IFE.02.CEA-01 – Magnetized ICF

WP1 deliverables

1st year (2024):

D1.1 - Extend the cylindrical implosions under B-fields from 15 kJ (at Omega) up to 300 kJ laser drive (at NIF)

Magnetized shot shows an increase of primary neutron yield and implosion stability

Observed Ar H-like lines are compatible with $T_e \approx$ 1400 eV in the core (when external B-field is applied)

– presented at EPS CPP 2024 (J.J. Santos, invited talk; A. Bordon, poster) and at APS DPP 2024 (E. Rovere, talk)

D1.2 - Characterize **ion temperature** (from primary neutron yield) and the **amplitude and topology of the compressed B-field** (from secondary neutrons) at NIF

Secondary neutron yield not observed in the NIF shots of June 2024, compatible with measured CR ~ 12

Improved target (thicker shell, denser fuel) and laser-drive (pulse shaping) designs for the follow-up NIF shots in April 2025

2nd year (2025):

D1.3 - **Report on the improved spectroscopic techniques**

Dopant K-shell emission spectroscopy successfully characterizes dense, magnetized, laser-driven plasmas, led to **quantitative estimates of the imploded core plasma conditions**: at OMEGA, 50% increase in core temperature in magnetized shots consistent with compressed B-field ~ 10 kT ()

Dual-dopant techniques (Ar + Ne and Ar+Kr in respectively cylindrical and spherical implosions) are being submitted

D1.4 - **Magnetized cylindrical implosion experiment at LMJ** with 300 kJ laser drive and LDC targets for generating the seed B-field

Postponed to 2027; Design improvement is ongoing for both the implosions and the seed B-field driving with LDC

D1.5 – For NIF experiments: **core temperature profiles from dual-dopant K-shell emission spectroscopy**

Objective transferred for the LMJ experiment, given the lower CR (more stable) with the novel NIF targets

and **B-field compressibility from angularly resolved spectra of secondary neutrons emission**

How accurate are the coefficients of energy transport ?

Transport coefficients link the **electric and magnetic fields** to **currents** and **temperature gradients**

B-field advection velocity :

$$\underline{v}_B = \underline{v} \underbrace{- \gamma_\perp \nabla T_e}_{\text{Nernst}} \underbrace{- \gamma_\wedge (\hat{\underline{b}} \times \nabla T_e)}_{\text{Cross-gradient-Nernst}} \underbrace{- \frac{\underline{j}}{en_e}(1+\delta_\perp^c) + \frac{\delta_\wedge^c}{en_e}(\underline{j} \times \hat{\underline{b}})}_{\text{Hall terms}}$$

and the **heat flux** to **temperature gradients**

Heat flux :

$$\underline{q}_\kappa = \underbrace{- \kappa_\parallel \nabla_\parallel T_e}_{\text{Conduction along B-field lines}} \underbrace{- \kappa_\perp \nabla_\perp T_e}_{\text{Suppressed conduction perpendicular to B}} \underbrace{- \kappa_\wedge \hat{\underline{b}} \times \nabla T_e}_{\text{Righi-Leduc heat flow}}$$

Different theories predict different coefficients

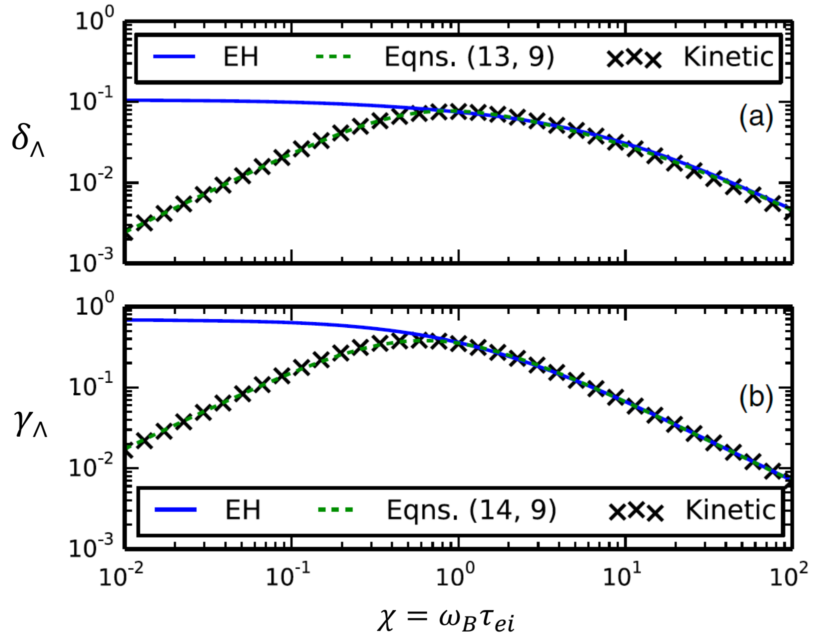

Sadler *et al.*, Phys. Rev. Lett. **126**, 075001 (2021)

Strong need to compare to experimental measurements, which are challenging;

There is very little experimental data…

Building up experimentally-verified transport coefficients

The transport coefficients stem from e-i and e-e collisions (micro-physics)

For weakly coupled plasmas, they essentially depend on :

- the **Hall parameter** $\chi = \boldsymbol{\omega_B \tau_{ei}}$ (electron magnetisation)
- and the **Knudsen parameter** $\boldsymbol{\lambda_{ei}/L_T}$ $(L_T = T/\nabla T)$

Goals:

- Medium-scale **experiments with simplified geometries** covering a broad range of magnetization and locality levels
- **Collect data on broad ranges of plasma parameters to infer transport coefficients** (heat transport, B-field advection and diffusion)
- **Benchmark the models and simulations**, and therefore provide a robust guidance to the experimental design of the larger scale (magnetized) ICF experiments

Validity domains of various kinetic models in the Knudsen - Hall parameter space

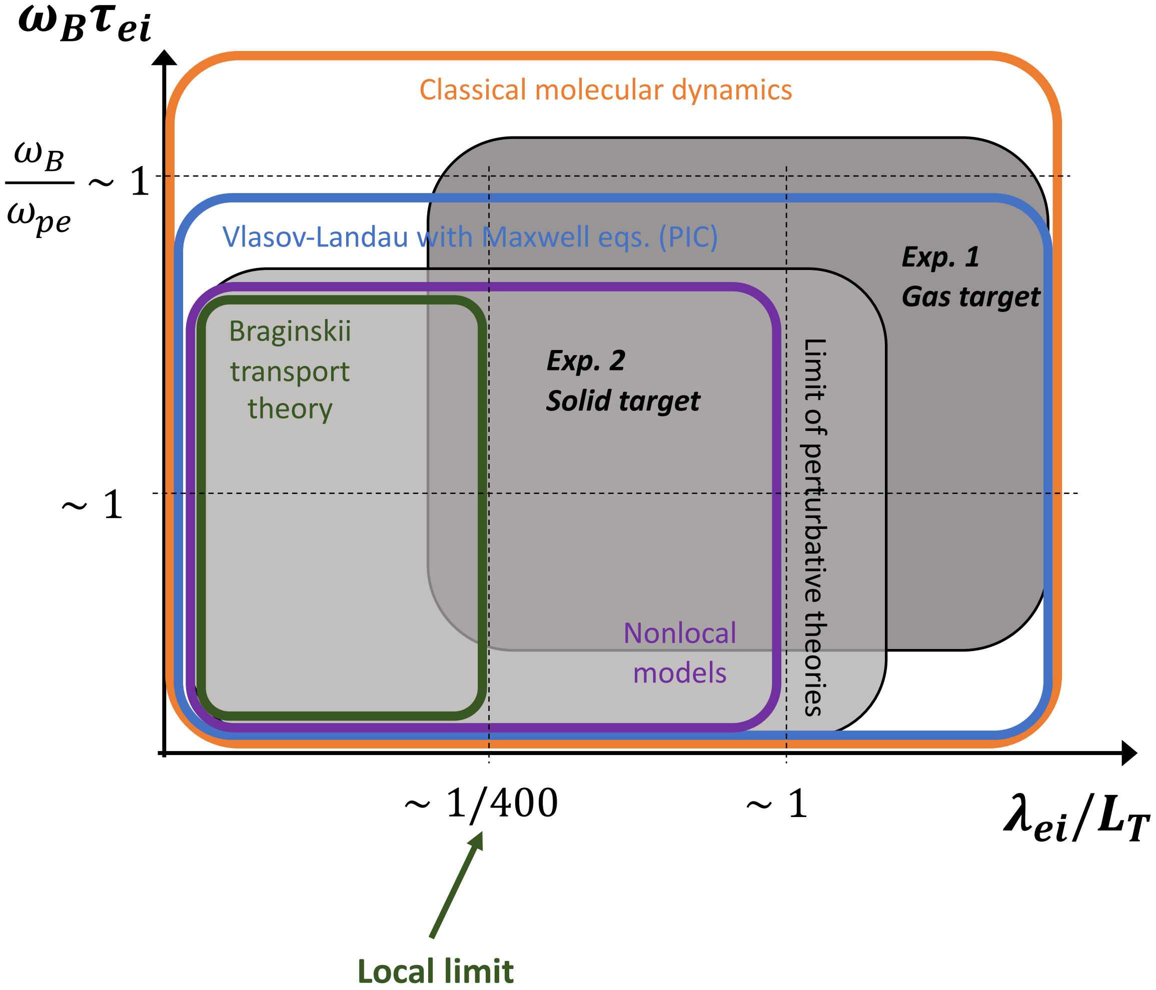

Microphysics of heat transport at LULI

Two experiments with low density gas jets and an external B-field

Platform for under-dense plasma characterization in the presence of a B-field of up to 20 T

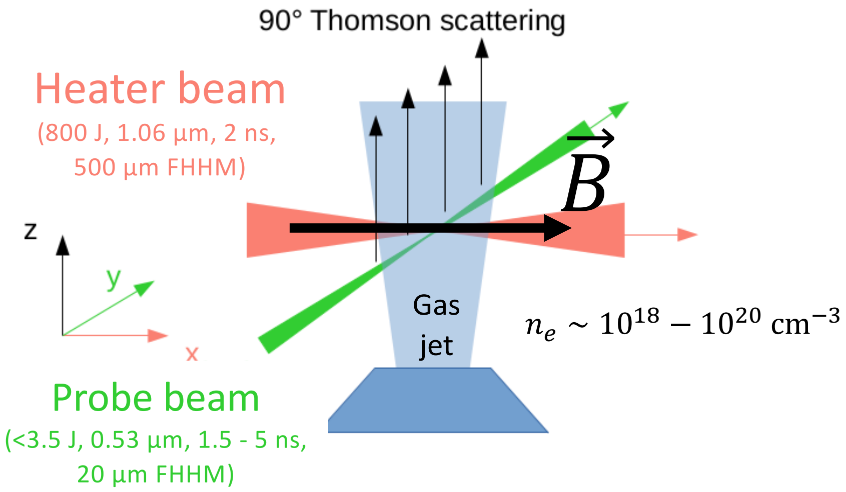

Heater beam
(800 J, 1.06 µm, 2 ns, 500 µm FHHM)

Probe beam
(<3.5 J, 0.53 µm, 1.5 - 5 ns, 20 µm FHHM)

Optical Thomson Scattering (OTS) spectra give access to local plasma parameters

Ion spectrum

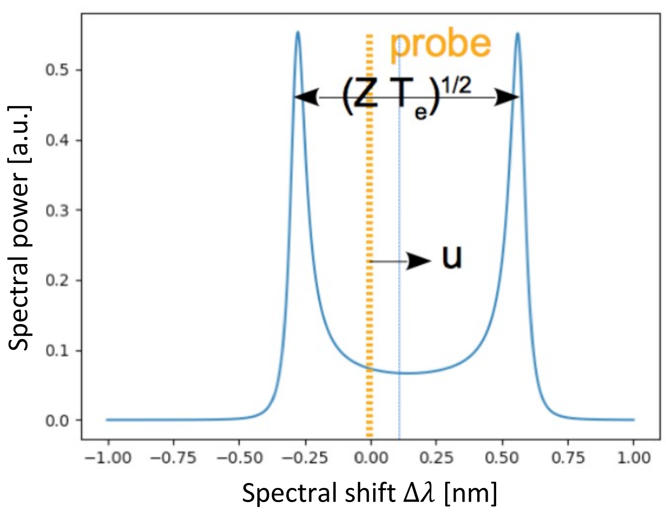

Electron spectrum

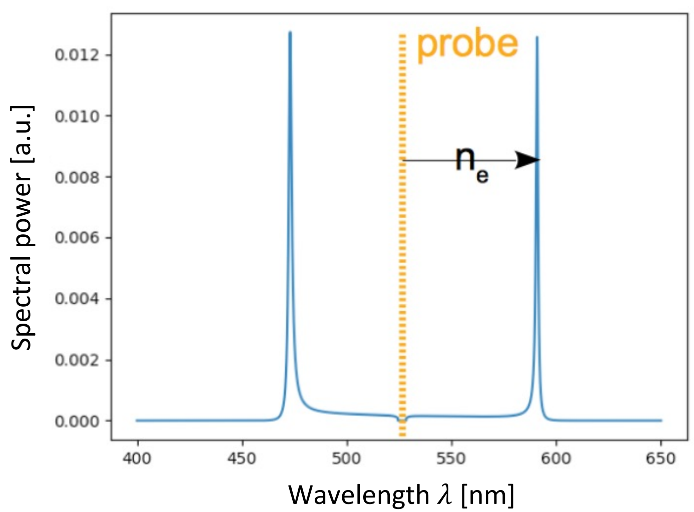

Microphysics of heat transport at LULI

Look at thermal transport in gas jets using Thomson scattering

Multiple Thompson Scattering channels yield simultaneously both electronic and ionic spectra

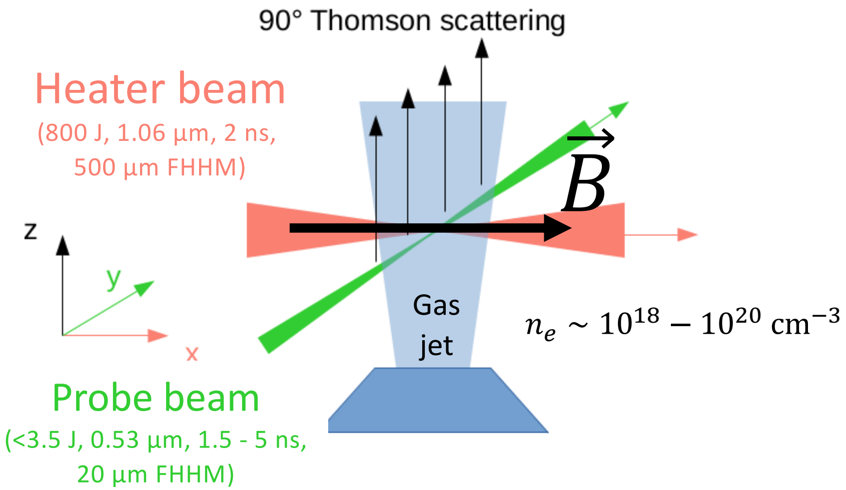

90° Thomson scattering

Heater beam

(800 J, 1.06 µm, 2 ns,
500 µm FHHM)

Probe beam

(<3.5 J, 0.53 µm, 1.5 - 5 ns,
20 µm FHHM)

Gas jet

$n_e \sim 10^{18} - 10^{20}\ \mathrm{cm}^{-3}$

With external B-field up to 20 T (‖ laser axis) we could explore:

- $\chi = \omega_B \tau_{ei}$ between 10 and 100
- $\beta = \frac{p_{th}}{p_B}$ between 1 and 30

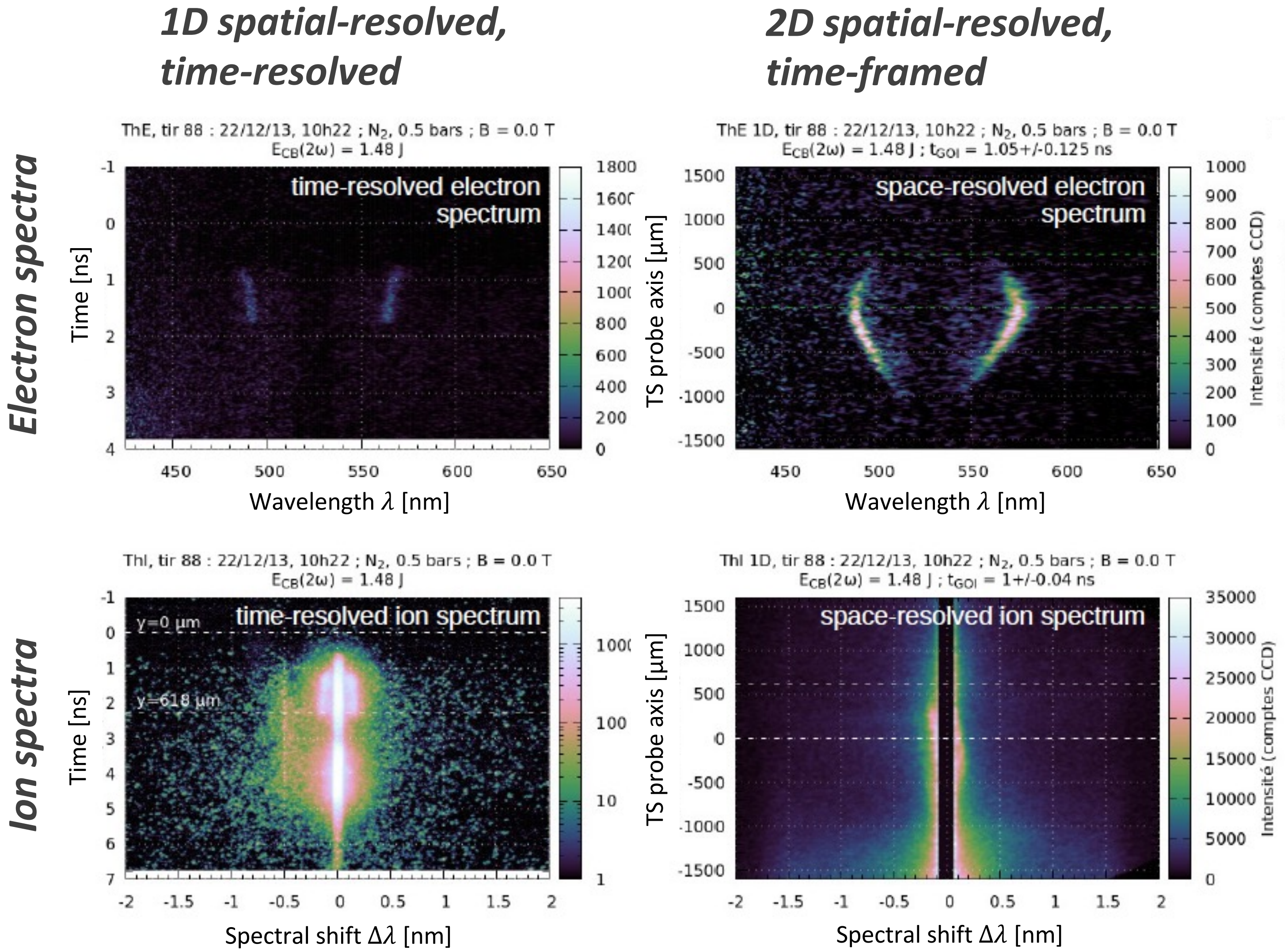

1D spatial-resolved, time-resolved

2D spatial-resolved, time-framed

Electron spectra

Ion spectra

Spectra from non-magnetized shots compared to synthetic spectra

Both electron and ion synthetic spectra are sensitive to hydro modeling options: flux limiter, probe beam effects…

Rad-hydro simulations with all laser beams

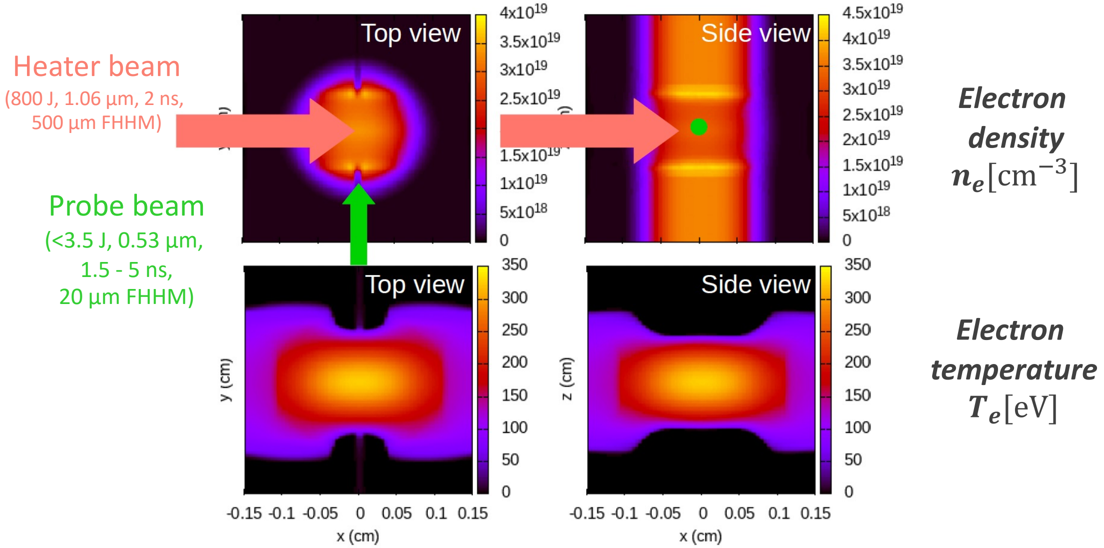

Spatially resolved electron spectra at 1 ns - H_2 14 bars

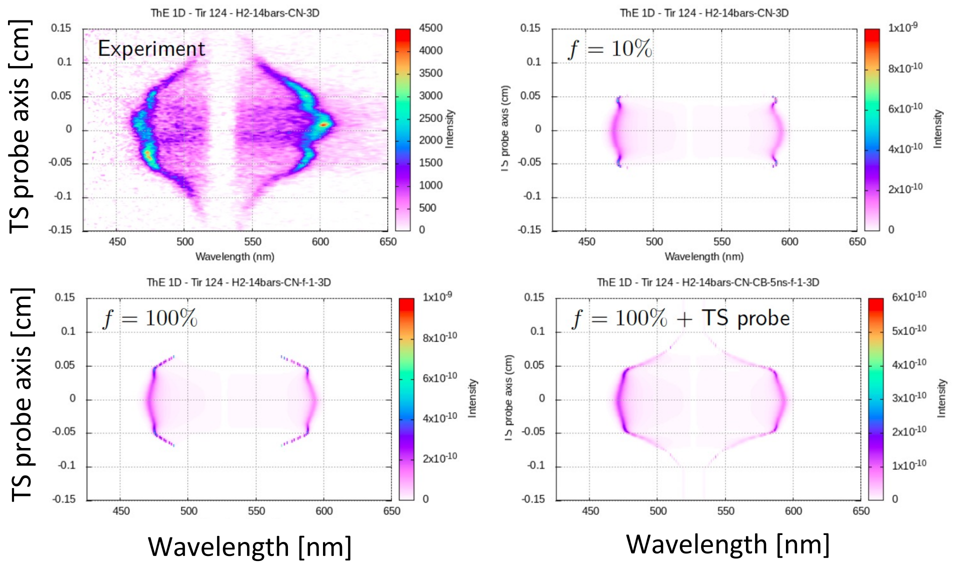

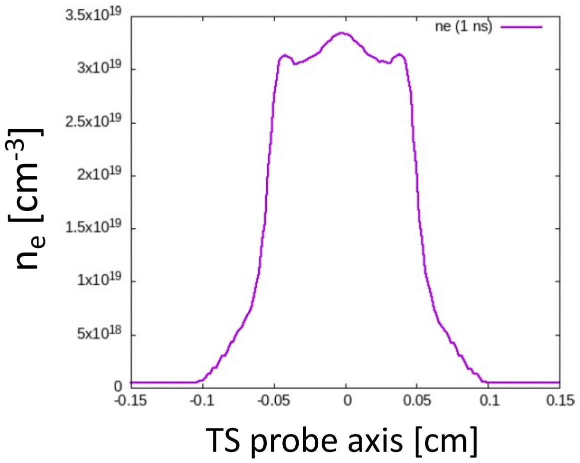

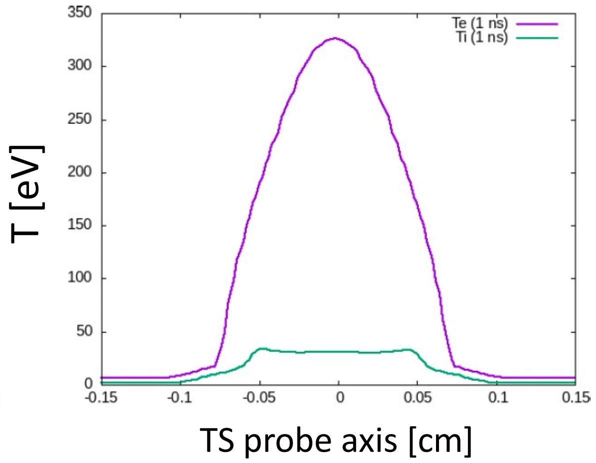

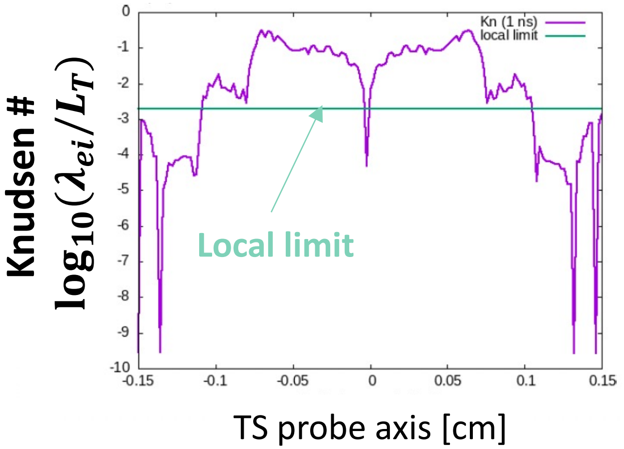

Plasma parameters (steep $\vec{\nabla}T_e$) indicate non local electron thermal conduction

Microphysics of heat transport at LULI

Higher densities measurements with solid targets and X-ray absorption

LULI experimental sketch for Feb-March 2025

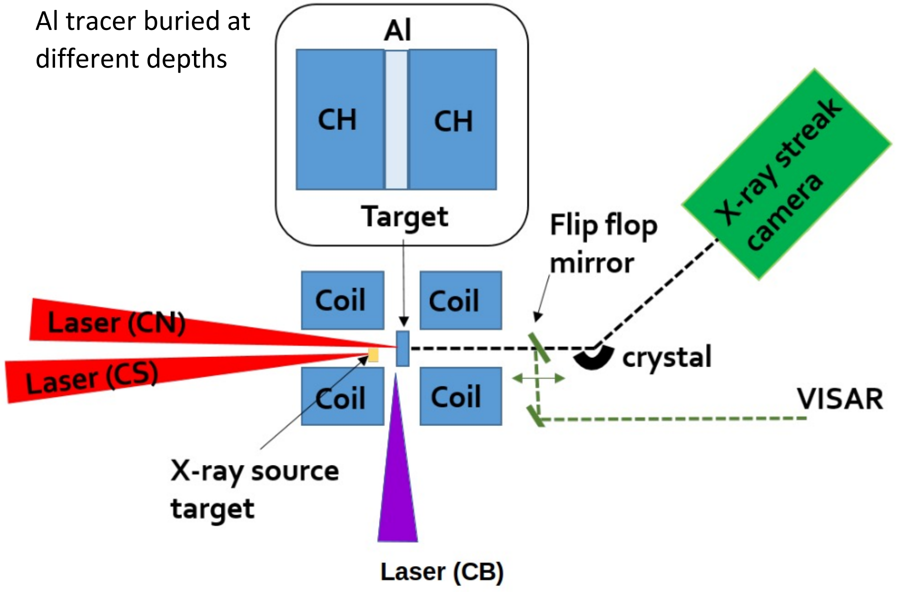

Time-resolved X-ray absorption spectra will measure electron temperature at different depths and times, with and w/o the external B-field

\+ **Laser-plasma instabilities** assessed from time- and spectral-resolved **Raman and Brillouin backscattered energies**

20 T B-field is expected to strongly modify thermal conductivity

Temperature and density profiles at 0.8 ns

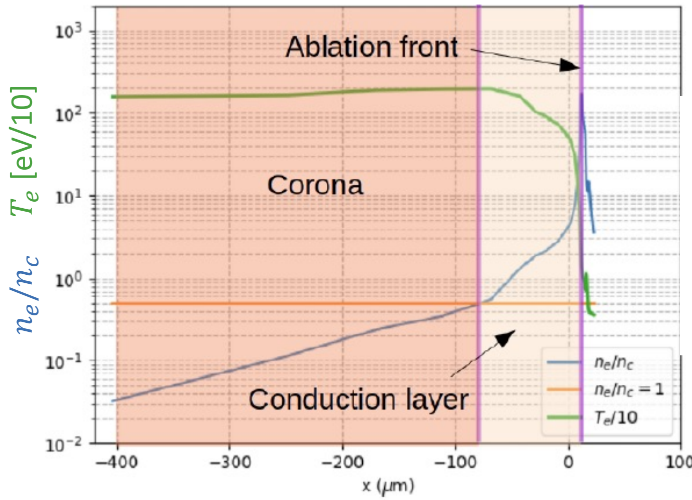

Thermal conductivity profiles at 0.8ns

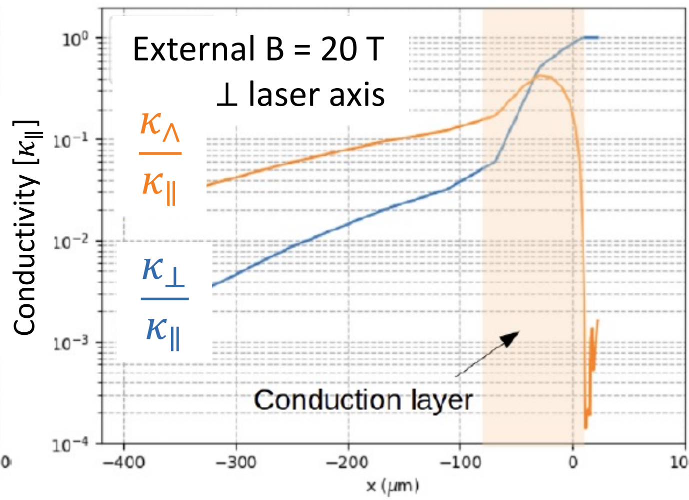

… and therefore the heat diffusion length $l^2 \sim \kappa t / C_V$

Simulation predictions for
CH 15 µm / Al 0.3 µm / CH 2 µm

Al 1s-2p absorption spectra

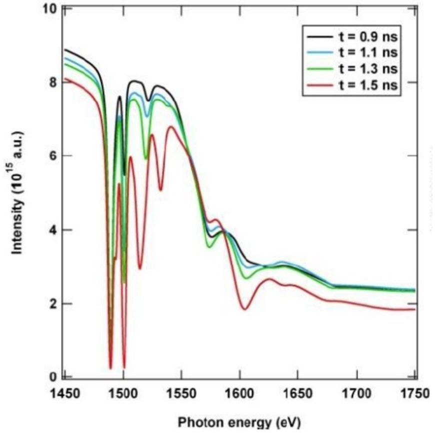

Al-layer average temperature

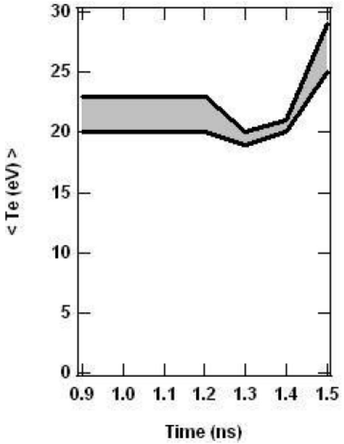

ENR-IFE.02.CEA-01 – Magnetized ICF

WP2 deliverables

1st year (2024):

D2.1 - Electron energy flux measurements in a broad range of plasma parameters and magnetizations

Two experiments with low density gas jets and B-field up to 20 T provided vast collection of data

Extraction of plasma parameters from TS data being improved (out of equilibrium $f_\alpha(\vec{v})$)

– presented at IFE workshop at EU-XFEL, June 2024 (P. Loiseau, talk)

2nd year (2025):

D.2.2 – Broaden the scanned parameters with solid targets and explore XFEL probing

Experiment with solid targets and laser-driven X-ray probing (absorption spectroscopy), Feb-March 2025 at LULI

XFEL experiment would need $\gtrsim$ 100 J ns laser and $B_0 \gtrsim$ 20 T; being thought of, **realization likely to slide beyond 2025**

D2.3 - Self-consistent simulations of heat transport covering a broad range of the Knudsen - Hall parameter space

Ongoing with TROLL and Aladin for low-density plasmas case, with benchmarking data from the gas jets experiments

D2.4 - Plasma particle dynamics in highly magnetized plasmas from N-body classical MD simulations

Heat transport modeling through MD and PIC simulations is ongoing

D2.5 - Incorporation of evolved transport models/coefficients to extended-MHD codes and improved simulations of large-scale implosion (laser fusion) experiments

Foreseen improvements on the design, interpretation and predictability of ICF and magnetized ICF experiments and on the modeling of astrophysical plasmas

ENR-IFE.02.CEA-01 – Magnetized ICF

Requested administrative and budget changes

1st year (2024):

1) **Total Res. (Eq./OGS 40% standard) of 83.75 kEUR should be shifted to 2025**.
Motivation: The LMJ experiment initially scheduled to 2025 was re-scheduled in 2026-27 by the facility (decision communicated to the users in July 2024). Therefore the target production was shifted from 2024 to 2025.

2) Open positions in 2024 at CIEMAT were filled as follows:
- **Ehret Michael** (CLPU), 2 PM
- **Henares José-Luis** (CLPU), 2 PM covered by other means than the project budget

3) 2024 implementation at NCSRD should be changed to:
- Fitilis Ioannis (HMU), **3 PM** (instead of 2.5 PM)
- Vlachos Christos (HMU), **3 PM** (instead of 3.5 PM)

4) 2024 implementation at CEA :
- **Barlow Duncan** should be replaced by **Caetano de Sousa Meirielen** (CNRS), 2 PM.

5) 2024 implementation at UKAEA shows a wrong person:
- **Aalto Timo** (I don’t even know this person) should be replaced by **Jeremy Chittenden** (2 PM covered by other means than the project budget).

2nd year (2025):

1) Incorporation of **83.75 kEUR in Total Res. (Eq./OGS 40% standard)**, shifted from 2024

2) Open positions in 2025 at CIEMAT were filled as follows:
- **Henares José-Luis** (CLPU), 2 PM
- **TBD** (CLPU), 2 PM covered by other means than the project budget

3) 2025 implementation at NCSRD should be changed to:
- Fitilis Ioannis (HMU), **2.5 PM**
- Tazes Ioannis (HMU), **3.5 PM** (instead of Vlachos Christos)

4) 2024 implementation at CEA :
- **Barlow Duncan** should be replaced by **Caetano de Sousa Meirielen** (CNRS), 2 PM.

5) 2025 implementation at UKAEA shows a wrong person:
- **Aalto Timo** should be replaced by **Jeremy Chittenden** (2 PM covered by other means than the project budget).

Thank you !

Work supported by:

- ***EUROfusion consortium***
  Grant Agreement Nos. 633053 and 101052200
- ***NNSA/NLUF, USA***
  Grant DE-NA0003940
- ***DOE Office of Science, USA***
  Grant DE-SC0022250
- ***Lawrence Livermore National Laboratory, USA***
  Contract No. DE-AC52-07NA27344
- ***Spanish Ministry of Science and Innovation***
  Research Grant No. PID2019-108764RB-I00
- ***Agence Nationale de la Recherche (ANR), France***
  Project ANR-22-CE30-390 0044
- ***Investment for the Future Program, IdEx, Université de Bordeaux/GPR LIGHT***